UNIVERSITY OF HELSINKI REPORT SERIES IN ASTRONOMY

No. 7

Radiative transfer modelling of interstellar clouds

Tuomas Lunttila

Academic dissertation

Department of Physics
Faculty of Science
University of Helsinki
Helsinki, Finland

To be presented, with the permission of the Faculty of Science of the University of Helsinki, for public criticism in Auditorium A110 of Chemicum at Kumpula Campus on 30 November 2012, at 12 o'clock noon.

Helsinki 2012

ISSN 1799-3024 (printed version)
ISBN 978-952-10-8080-7 (printed version)
Helsinki 2012
Helsinki University Print (Unigrafia)

ISSN 1799-3032 (pdf version)
ISBN 978-952-10-8081-4 (pdf version)
ISSN-L 1799-3024
http://ethesis.helsinki.fi/
Helsinki 2012
Electronic Publications @ University of Helsinki (Helsingin yliopiston verkkojulkaisut)

Tuomas Lunttila: **Radiative transfer modelling of interstellar clouds**, University of Helsinki, 2012, 51 p.+appendices, University of Helsinki Report Series in Astronomy, No. 7, ISSN 1799-3024 (printed version), ISBN 978-952-10-8080-7 (printed version), ISSN 1799-3032 (pdf version), ISBN 978-952-10-8081-4 (pdf version), ISSN-L 1799-3024

Classification (INSPEC): A9530J, A9575P, A9840B, A9840J, A9840K, A9840L
Keywords: radiative transfer, interstellar medium, molecular clouds, star formation, molecular spectral lines, dust continuum, scattering

Abstract

Almost all information on astrophysical objects is obtained through observation of electromagnetic radiation. The observed radiation has been altered in interactions with matter, and understanding the transport of radiation is a key prerequisite for understanding the physical conditions in the observed objects. The transport of radiation is described by the radiative transfer equation. Owing to its complex nature, solving the radiative transfer equation is difficult, and it is usually necessary to resort to numerical calculations. In this thesis, the focus is on the modelling of radiation transport in interstellar clouds. The dense gas and dust in interstellar clouds scatter, absorb, and emit radiation, and understanding the radiative transfer effects is crucial in the interpretation of observations.

Four of the five articles that are contained in this thesis concern various applications of radiative transfer modelling. Two articles focus on the modelling of spectral line radiation. We study the use of OH Zeeman splitting observations in the determination of magnetic field strengths in molecular clouds. The role of magnetic fields in the process of star formation is still largely an open question with two competing models: the turbulence dominated scenario where magnetic fields are weak, and the ambipolar diffusion driven model with stronger magnetic fields. By combining magneto-hydrodynamical calculations with radiative transfer simulations, we show that the turbulence dominated scenario is consistent with the observed magnetic field strengths.

Two articles concern the dust radiative transfer. We study the dust density distribution and grain properties in the dust envelope surrounding the carbon star IRC +10 216. By modelling the surface brightness distribution of the scattered light in the dust envelope, we can infer the mass-loss history of the star and improve models of newly formed dust grains. In another article we use magneto-hydrodynamical calculations and radiative transfer simulations to study the reliability of cloud core mass estimates. Observations of dust thermal emission at the far-infrared and submillimetre wavelengths are commonly used to determine the masses of molecular cloud cores. By constructing synthetic observations of a model cloud and comparing the estimated masses to the true masses that are obtained directly from the cloud model, we can determine the robustness of mass estimates.

Instead of focusing on the applications of radiative transfer modelling, one article describes new numerical methods for efficient radiative transfer simulations. We describe new algorithms for radiative transfer on hierarchical grids. The new algorithms, in particular the use of sub-iterations, are faster by a factor of several compared to the old methods.

Acknowledgements

The work carried out for this thesis was done at the Observatory of the University of Helsinki and, after the merging of the departments at the beginning of 2010, at the Department of Physics.

I am deeply grateful to my thesis supervisor, Docent Mika Juvela. Without his indispensable guidance and support I could not have written this thesis. I would like to thank Professor Emeritus Kalevi Mattila and Docent Jorma Harju for their advice and support. I am also thankful to the other members of the Interstellar medium and star-formation Research group for providing a stimulating research environment, and the rest of the staff at the Observatory and later at the division of Geophysics and Astronomy of the Department of Physics.

I am indebted to the pre-examiners Professor Juri Poutanen and Dr. Joni Tammi for their valuable comments on the thesis. I am also grateful to Dr. habil. Jürgen Steinacker for agreeing to be the Opponent, and to Professor Karri Muinonen for taking the role of the Custos.

Last but not least, I am thankful to my family for their support.

The thesis work was supported financially by the Vilho, Yrjö, and Kalle Väisälä Foundation, the Magnus Ehrnrooth Foundation, the Finnish Graduate School in Astronomy and Space Physics, and the Academy of Finland.

List of publications

Paper I: T. Lunttila and M. Juvela, 2007, "Inferring the dust properties and density distribution in the outer envelope of IRC +10 216 from scattered Galactic light", Astronomy & Astrophysics, 470, 259

Paper II: T. Lunttila, P. Padoan, M. Juvela, and Å. Nordlund, 2008, "The Super-Alfvénic Model of Molecular Clouds: Predictions for Zeeman Splitting Measurements", The Astrophysical Journal Letters, 686, 91

Paper III: T. Lunttila, P. Padoan, M. Juvela, and Å. Nordlund, 2009, "The Super-Alfvénic Model of Molecular Clouds: Predictions for Mass-to-Flux and Turbulent-to-Magnetic Energy Ratios", The Astrophysical Journal Letters, 702, 37

Paper IV: T. Lunttila and M. Juvela, 2012, "Radiative transfer on hierarchial grids", Astronomy & Astrophysics, 544, A52

Paper V: J. Malinen, M. Juvela, D. C. Collins, **T. Lunttila**, and P. Padoan, 2011, "Accuracy of core mass estimates in simulated observations of dust emission", Astronomy & Astrophysics, 530, A101

Contents

1 Introduction **1**

1.1 Interstellar medium 1

1.2 Interstellar dust 2

1.3 Molecular clouds and the formation of stars 5

2 Radiative transfer in interstellar clouds **7**

2.1 Radiative transfer equation 7

2.2 Numerical solution 9

2.2.1 Discretisation 9

2.2.2 Solving the linear equation 10

2.2.3 Iterative solution of the full problem 12

2.3 Applications of radiative transfer calculations 13

3 Simulations of dust continuum radiation **15**

3.1 Interaction of dust grains with the radiation field 15

3.1.1 Absorption and scattering 15

3.1.2 Emission from the dust grains 16

3.2 Applications 18

3.2.1 Estimating the column density using dust thermal emission . . 18

3.2.2 Observations of scattered light 21

4 Simulations of Zeeman splitting **24**

4.1 Magnetic fields in star-formation 24

4.2 Observing the magnetic fields 26

4.3 Zeeman splitting of spectral lines 27

4.4 Determining the magnetic field from Zeeman splitting observations . . 32

5 Summary of the publications **36**

5.1 Paper I 36

5.2 Paper II 38

5.3 Paper III 39

5.4 Paper IV 40
5.5 Paper V 41

6 Conclusions and future prospects **43**

Bibliography **44**

Chapter 1

Introduction

This thesis is focused on the study of the interstellar medium (ISM). The articles included in the thesis span almost the whole life-cycle of the ISM from the formation of dust grains in outflows from giant stars to dense prestellar cores where a new generation of stars is born. An important unifying theme in the thesis is the use of radiative transfer calculations. The calculations are needed to relate the observed radiation to physical conditions in the observed object. Computing the transport of radiation numerically is difficult, and we also discuss methods for solving the problem efficiently.

The thesis begins with a brief overview of the interstellar matter and star-formation. For a more detailed discussion we refer to the books Scheffler & Elsaesser (1987) and Stahler & Palla (2005), and the review article McKee & Ostriker (2007). Chapter 2 is an introduction to the radiative transfer equation (RTE) that governs the transport of radiation, and a review of various methods that can be used to solve the equation. Chapter 3 presents some applications of dust continuum radiative transfer calculations. Chapter 4 focuses on spectral lines, in particular on their use in the estimation of magnetic fields in molecular clouds. Chapter 5 summarises the publications included in this thesis. Finally, conclusions and some prospects for future work are given in chapter 6.

1.1 Interstellar medium

The existence of dark patches on the sky, apparently devoid of stars, was already observed in the 18th century by William Herschel. At that time, they were believed to be truly "holes in the heavens". Only in the early 20th century, the "holes" were understood to be dark clouds that block the light from background stars. In 1930 Trumpler showed by studying the apparent sizes of open clusters that even the apparently transparent parts of the interstellar space are filled with an obscuring medium.

Today the space between the stars is known to be filled with an interstellar medium (ISM), a mixture of gas and small dust grains, comprising 10–15 % of the total baryonic mass of the Milky Way. Approximately one percent of the interstellar matter is in the form of dust grains, while the rest is in the gas phase. The gas is mostly hydrogen and helium (≈ 74 % and ≈ 24 % by mass, respectively), with only a small fraction of heavier elements. Nevertheless, the interplay of dust and gas leads to a rich chemistry, and more than a hundred molecular species have been identified in the ISM.

The ISM consists of several phases (McKee & Ostriker, 1977). Most of the volume is filled with a hot ($T \sim 10^6$ K), low density (particle density $n \sim 10^{-3}$ cm^{-3}) ionised gas called the hot ionised medium. The next largest fraction by volume is taken by a cooler ($T \sim 10000$ K) and denser $n \sim 0.3$ cm^{-3} warm phase. The warm gas exists in both neutral and ionised components. Approximately 4 % of the volume is taken by the cold neutral medium ($T \sim 80$ K, $n \sim 50$ cm^{-3}). A small fraction, $\lesssim 1$ % of the volume is filled with cold molecular gas. However, owing to its high density, $n \sim 300$ cm^{-3}, the molecular phase contains a substantial fraction (~ 20 %) of the total gas mass. In the densest cores of molecular clouds the density can reach values of $n > 10^5$ cm^{-3}, but the cores only occupy a very small fraction of the cloud volume. Temperature of the molecular gas is typically ≈ 20 K, but in the densest parts of molecular clouds the temperature can be less than 10 K (Harju et al., 2008).

The ISM is not static. Cold, dense cores in molecular clouds collapse to form stars. The nuclear reactions in the stellar cores change the abundances of elements. The stars return some of the material back to the ISM during their red giant and asymptotic giant branch phases in strong stellar winds, and because (a part of) the matter has been processed in nuclear reactions, it is enriched in heavy elements. Massive stars have strong stellar winds throughout their lifetimes, and end their lives in supernova explosions that disperse the outer layers of the star to the ISM. Most of the mass returned to the ISM comes from stellar winds of relatively low mass giant stars. However, the massive stars produce most of the heavy elements. Massive stars are also important because they inject energy to the ISM through their strong stellar winds and supernova explosions.

1.2 Interstellar dust

Although the dust comprises only approximately one percent of the total mass of the ISM, it is responsible for some of the most conspicuous objects in the night sky. Small dust grains are very effective at blocking the light at visible wavelengths, and dark clouds such as the Horsehead nebula are caused by dust extinction (Fig. 1.1). Dust grains also scatter (reflect) light, and if an interstellar cloud is illuminated by a

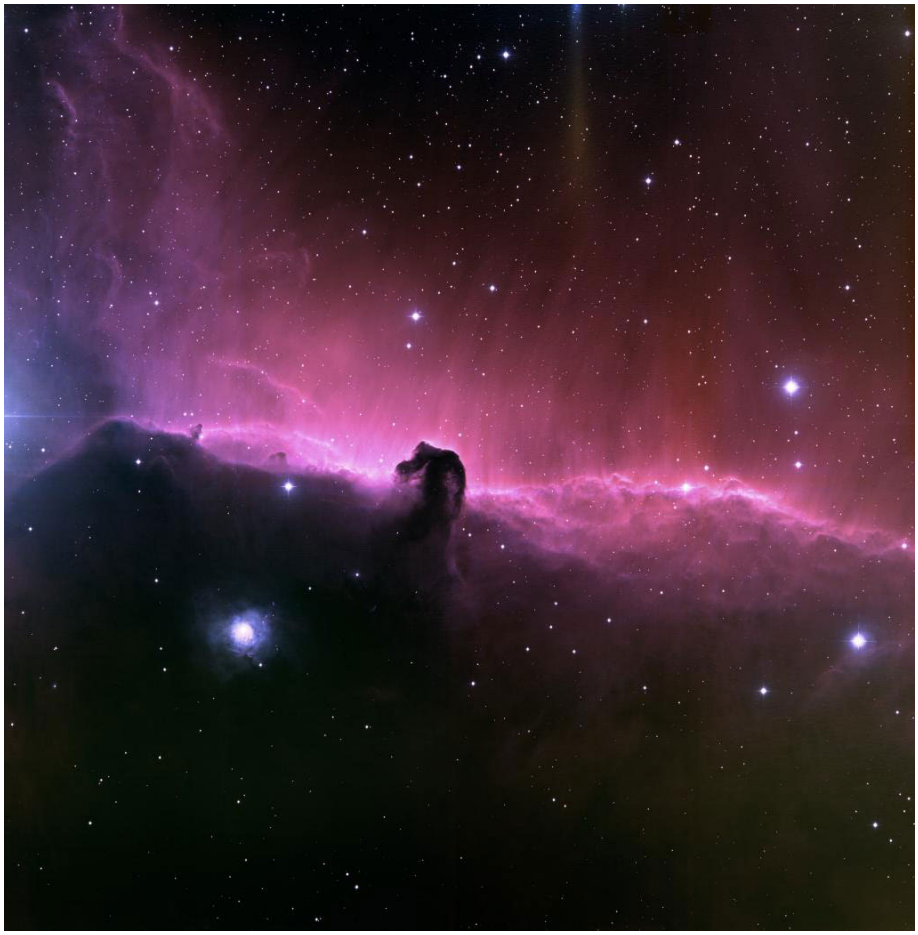

Figure 1.1: The dark Horsehead nebula is seen silhouetted against the IC434 star-forming region. Dust grains in the Horsehead nebula block the hydrogen Hα radiation that is coming from the HII region in the background. The image is a composite of Hα (red), oxygen [OIII] (green) and sulphur [SII] (blue) emission line images. The images were taken with the 0.9 m NSF telescope on Kitt Peak. Image credit: T.A.Rector (NOAO/AURA/NSF) and Hubble Heritage Team (STScI/AURA/NASA).

nearby star, a reflection nebula such the ones surrounding the Pleiades can be seen (Fig. 1.2).

Dust is very useful in the study of the structure of the ISM, in particular the molecular clouds. The main gas component of the molecular clouds, molecular hydrogen (H_2), is difficult to detect directly owing to its lack of suitable spectral lines that would be excited in the normal ISM conditions, and spectral lines of other tracer molecules, principally CO, must be used to study the clouds. However, the abundances of molecules depend on complex chemical reaction networks, and it may be difficult to interpret molecular line observations. Interstellar dust provides another method to study the ISM. The dust interacts strongly with the ultraviolet-visible-

Figure 1.2: Red-green-blue composite image of the Pleiades open cluster. Nebulosity is caused by scattering of starlight from dusty clouds surrounding the bright stars of the cluster. The images were taken with the 1.22 m Samuel Oschin telescope at the Palomar observatory. Image credit: NASA, ESA and AURA/Caltech.

near-infrared light, causing extinction of the background starlight, and scattering the light impinging on the cloud. Dust grains also emit thermal radiation at the far-infrared and sub-millimetre wavelengths. Because the column density of dust has been found to be well correlated with the hydrogen column density (Bohlin, 1975; Bohlin et al., 1978), studies of dust can provide information on the structure of the molecular cloud.

Of course, to apply the methods, it is necessary to know the properties of dust grains. The information about the dust grains is obtained mainly from the study of extinction curves, i.e. how the intensity of starlight decreases as a function of wavelength. The general shape of the curve is a good probe of the grain size distribution, while absorption bands can be used to infer the chemical composition. Other constraints are given by observations of scattering, thermal emission, and polarisation, and the abundances of elements available for building dust grains. Studies indicate that interstellar dust grains are very small, with a typical grain radius $a \sim 0.1$ μm. However, a continuous distribution of grain sizes is needed to fit the constraints. A widely used model by Mathis, Rumpl, and Nordsieck (Mathis et al., 1977) adopts a $N_d \propto a_d^{-3.5}$ distribution with cutoffs at 0.005 μm and 0.35 μm; more recent studies (e.g. Weingartner & Draine, 2001; Draine & Li, 2007; Compiègne et al., 2011)

have added details, but the general picture is similar. Two grain populations with distinct compositions are needed to explain the extinction curve data: carbonaceous grains consisting mainly of amorphous carbon, which form in carbon-rich outflows, and silicate grains, which condense in oxygen-rich environments. Recent models also include polyaromatic hydrocarbon (PAH) molecules. Dust properties are not constant throughout the Milky Way. In dense clouds the grain size increases because of dust coagulation and the formation of ice mantles on the dust grains (Ossenkopf, 1993; Ossenkopf & Henning, 1994).

Despite the low abundance of dust compared to gas, it plays an important role in interstellar chemistry. Many chemical reactions, most notably the formation of H_2 (Hollenbach & Salpeter, 1971), take place on the surfaces of dust grains. Dust grains also effectively block ultraviolet radiation, thereby shielding molecules from photodissociation (van Dishoeck & Visser, 2011). Furthermore, dust is important for the thermal balance of molecular clouds (Doty & Neufeld, 1997). Thermal far infrared radiation from dust grains cools the dense cores of molecular clouds, where cooling by spectral line radiation is ineffective because of high optical depth.

1.3 Molecular clouds and the formation of stars

The molecular gas in the Milky Way is largely concentrated in giant molecular cloud complexes. The clouds also account for most of the star-formation. Giant molecular clouds, such as the Orion and Taurus clouds, have typical sizes of a few tens of parsecs, masses of about a million times the Solar mass, and mean densities of a few hundred molecules per cubic centimetre. The giant clouds are not static structures. Individual clouds only survive for ~ 30 Myr before they are destroyed by the strong stellar winds from massive stars that have formed inside the cloud. The formation of molecular clouds from the diffuse and atomic phase is an actively researched topic that has benefitted from advancing super-computing capabilities. Recent results point toward a scheme where supersonic turbulence is the main factor driving the cloud formation and evolution. For reviews of the topic, see Mac Low & Klessen (2004) McKee & Ostriker (2007), and Ballesteros-Paredes et al. (2007).

Molecular clouds are very inhomogeneous and complex. They contain filaments and clumps on all observable scales in a hierarchical structure, where low density gas fills most of the volume, and the high-density structures enclose even denser structures. Characterisation and classification of these structures is currently an important area of research (e.g., Men'shchikov et al., 2010; Ward-Thompson et al., 2010; Arzoumanian et al., 2011). Improving observational facilities have greatly increased the amount of data available to researchers, and the development of computer algorithms to extract and classify structures from observational data automatically has been very

active (e.g., Williams et al., 1994; Rosolowsky et al., 2008b; Sousbie, 2011).

The formation of stars mainly takes place in dense cores inside molecular clouds. The cores are the smallest structures of the interstellar matter, and they have sizes of ~ 0.1 pc and densities of more than 10^4 cm^{-3} (Bergin & Tafalla, 2007). Star-forming molecular clouds that are close enough for individual cores to be identified have been found to contain several hundreds of cores (Enoch et al., 2008; Rosolowsky et al., 2008a). Inside the cores the density increases inwards, but otherwise the cores have very little internal structure.

According to current theories, the dense starless cores are the earliest precursors of forming stars. However, only a subset of cores collapse to form stars. Other cores are not gravitationally bound, and they will eventually disperse to the surrounding molecular cloud (McKee & Ostriker, 2007). Transient dense structures are also seen in numerical simulations (Padoan & Nordlund, 2002). The dense structures that are gravitationally bound and will eventually collapse to form stars are called prestellar cores.

For details of the formation and collapse of dense cores we refer to reviews by Bergin & Tafalla (2007), McKee & Ostriker (2007), Ward-Thompson et al. (2007), and André et al. (2009). Here we focus on one hotly debated question: the influence of magnetic fields on the process of star-formation. In the past, the standard theory of the star-formation was the one of a slow process, where the magnetic field in the cloud core supports the core against collapse. Only after the magnetic flux had been removed, the collapse could proceed (Shu et al., 1987). The flux can be removed in a process called *ambipolar diffusion* (AD). The AD means that the neutral molecules and atoms drift under self-gravity relative to the ions and electrons, which are tied to the magnetic field (Fiedler & Mouschovias, 1992, 1993). As a consequence of the AD, the core loses magnetic flux until the field can not provide enough support against gravity, and a collapse ensues.

A more recent theory is that of a turbulence-dominated star-formation (Padoan & Nordlund, 1999, 2002). In this model the mean magnetic field is weak, and magnetic fields are not important for the regulation of the process of star-formation. In the model the turbulence is super-Alfvénic, meaning that the mean turbulent velocity is larger than the Alfvén velocity V_A:

$$V_A = \frac{\|\mathbf{B}\|}{\sqrt{4\pi\rho}}, \tag{1.1}$$

where $\mathbf{B}$ is the magnetic flux density and ρ is the density of the medium. We will discuss the subject in more detail in chapter 4.

Chapter 2

Radiative transfer in interstellar clouds

2.1 Radiative transfer equation

Almost all information about astrophysical objects is obtained through observation of electromagnetic radiation of different wavelengths. To understand the nature of observed targets, it is essential to know how the observed radiation is created, and how it is changed between its origin and the observer's instrument. In this section we will briefly review the RTE, which describes the transport of radiation. For a thorough discussion of the RTE, see Chandrasekhar (1950), Mihalas (1978), and Cannon (1985).

An accurate description of the transport of electromagnetic radiation through an interacting medium requires, in principle, solving the Maxwell's equations. However, this is unfeasible in a complex setting, such as a molecular cloud or a stellar atmosphere. Instead of Maxwell's equations, the RTE is commonly used to solve the problem of energy transport in an interacting medium. The RTE is usually derived phenomenologically by considering the transport of energy into and out of an infinitesimal volume (see the references at the beginning of this section). However, the RTE can be derived from first principles starting from Maxwell's equations, at least in some simplified cases (see Mishchenko (2008) and references therein for a thorough discussion).

The RTE describes the behaviour of the (specific) intensity I as a function of position, direction, frequency, and time, i.e., $I = I(\mathbf{x}, \vec{k}, \nu, t)$. We note that in the general case the specific intensity is described by a 4×1 matrix (a column vector) $\mathbf{I}$ that is known as the Stokes vector: $\mathbf{I} = [I, Q, U, V]^{\mathbf{T}}$. The components describe the polarisation of radiation: I is the specific intensity, parameters Q and U describe the linear polarisation, and V is the circular polarisation. However, with the exception of chapter 4 we only consider the specific intensity I.

The RTE can be formally written as a differential equation for the change of

intensity per infinitesimal length:

$$\frac{1}{c}\frac{\partial I}{\partial t} + \frac{\partial I}{\partial s} = -\kappa I + j, \tag{2.1}$$

where c is the speed of light, κ is the linear extinction coefficient (opacity), and j is the emission coefficient. In this thesis we only consider the static case where the time-derivative is very small and can be ignored. Then I can be obtained as

$$I(s) = I(s_0)e^{-\tau(s_0,s)} + \int_{s_0}^{s} e^{-\tau(s',s)} j(s')ds', \tag{2.2}$$

where

$$\tau(s', s) = \int_{s'}^{s} \kappa(x)dx \tag{2.3}$$

is the *optical thickness* between s' and s (here $s' < s$, so $\tau(s', s) > 0$). Equation (2.2) is known as the *formal solution* of the radiative transfer equation. If functions κ and j were known, solving I would be reduced to a simple integration along the rays. However, κ and j usually depend on I: $\kappa = f(I)$, $j = g(I)$. The full problem thus consists of solving equation (2.1) together with the equations for κ and j.

In the case of dust continuum radiative transfer, it is useful to write j as a sum of the scattered intensity j_s that is proportional to the intensity, and the true emission j_e:

$$\frac{dI}{ds} = -(\kappa_a + \kappa_s)I_\nu + j_s + j_e, \tag{2.4}$$

where we have written the opacity κ as a sum of absorption and scattering opacities κ_a and κ_s. The scattered intensity is given by

$$j_s(\vec{k}) = \kappa_s \int_{4\pi} K(\vec{k}, \vec{k'})I(\vec{k'})d\vec{k'}, \tag{2.5}$$

where K is the normalised scattering kernel ($\int_{4\pi} K(\vec{k}, \vec{k'})d\vec{k} = 1$ for all $\vec{k'}$), which describes how the direction of radiation is changed in the scattering process.

On the other hand, j_e is usually a non-linear function of the radiation intensity I. In the case of spectral line radiation, j_e depends on the population numbers of atomic and molecular energy levels (see, e.g., Cannon (1985)). In dust continuum calculations, j_e depends on the temperature of the dust grains. In either case, j_e can be written as

$$j_e = \kappa_a B_\nu(T), \tag{2.6}$$

where B_ν is the Planck function. In the case of spectral line radiation T is the excitation temperature of the transition, whereas for dust continuum T is the temperature of the dust grains. In the general case, also κ can depend on the radiation field. This is very important in spectral line radiative transfer, where level population numbers directly influence the opacity. In dust continuum calculations it has been common to

assume that κ does not depend on I. However, this is not strictly true, and modern dust models include a temperature-dependent opacity (Compiègne et al., 2011).

As an important special case, we note that if $I(s_0) = 0$ (i.e., there is no background radiation), scattering is negligible ($j_s \approx 0$), $B_\nu(T)$ is constant along the line of sight, and $\tau(s_0, s) \ll 1$ (cloud is optically thin), we get from (2.2), (2.3), and (2.6)

$$\begin{aligned} I(s) &= \int_{s_0}^{s} e^{-\tau(s',s)} j_e(s') ds' = B_\nu(T) \int_{s_0}^{s} e^{-\tau(s',s)} \frac{-\partial\tau}{\partial s'} ds' = B_\nu(T) \int_0^\tau e^{-\tau'} d\tau' \\ &= (1 - e^{-\tau}) B_\nu(T) \approx B(T)\tau. \end{aligned} \tag{2.7}$$

Thus, the intensity is directly proportional to the optical thickness of the cloud.

2.2 Numerical solution

A closed-form solution to the RTE can be obtained only in simple cases. Usually, it is necessary to resort to numerical methods.

We write the RTE together with the equations for κ and j_e as

$$\begin{aligned} I &= \Lambda j_e \\ j_e &= f(I) \\ \Lambda &= g(I), \end{aligned} \tag{2.8}$$

Here Λ is a linear operator that maps a given emission to the new radiation field, and f and g are functions that map the local radiation field to emission and opacity, respectively. Evaluating f and g may require, for instance, solving the rate equations for atomic transitions. Functions f and g are usually non-linear, and the system of equations (2.8) must be solved iteratively. Each iteration step typically requires the solution of a linear transfer problem, i.e., evaluating the formal solution given in equation (2.2). For the sake of clarity, we assume below that Λ does not depend on the radiation field, as is often case in dust continuum calculations.

2.2.1 Discretisation

For numerical solution of the RTE, a model has to be discretised so that it can be described in a finite computer memory. This is most commonly done by dividing the space into a finite number of cells. Inside each cell the physical quantities such as the density and the dust temperature are assumed to be constant. Similarly, also the frequency and, in some methods, the direction of the radiation are divided into a finite number of bins.

The choice of space discretisation depends on the details of the problem. For example, a spherically symmetric model can be described using only spherical shells, while for a complicated three dimensional structure a cartesian grid may be more suitable. Also more complicated schemes are possible (see, e.g., Ritzerveld & Icke,

2006). An accurate description of the structure often requires the inclusion of a large variety of scales. For instance, a model of a circumstellar disc may require a resolution of the order of a Solar radius near the star, while, to include the whole disc, the total extent of the model needs to be several hundred AU (e.g., Pinte et al., 2009). If a uniform cartesian three dimensional grid were used, hundreds of billions cells and tens of terabytes computer memory would be needed. To address this problem, several codes have been developed with support for adaptive resolution (e.g., Jonsson, 2006; Acreman et al., 2010). This means that the resolution on the (spatial) discretisation changes across the model, and the finest resolution is used only where it is needed. The use of an adaptive grid can decrease the number of cells in the model by several orders of magnitude.

The discretisation of the frequency space depends on the details of the problem. In line transfer calculations narrow bins are needed to capture the shapes of line profiles, while in continuum radiative transfer much wider frequency bins are usually sufficient. The angle discretisation depends on the solution algorithm, and in some methods an explicit discretisation is not needed.

In discretised form system (2.8) can be written as

$$\begin{aligned} \mathbf{I} &= \mathbf{\Lambda}'\mathbf{j_e} \\ \mathbf{j_e} &= \mathbf{f}(\mathbf{I}). \end{aligned} \tag{2.9}$$

Here $\mathbf{I}$ and $\mathbf{j_e}$ are $N_{\mathrm{cells}}N_{\mathrm{freq}}N_{\mathrm{dir}} \times 1$ matrices (column vectors) and $\mathbf{\Lambda}'$ is a $N_{\mathrm{cells}}N_{\mathrm{freq}}N_{\mathrm{dir}} \times N_{\mathrm{cells}}N_{\mathrm{freq}}N_{\mathrm{dir}}$ matrix. N_{cells}, N_{freq}, and N_{dir} are the number of cells, frequencies, and directions in the discretisation, respectively. In many cases, emission $\mathbf{j_e}$ only depends on the angle-averaged intensity $J = \frac{1}{4\pi}\int_{4\pi} I(\vec{k})d\vec{k}$, and the angular distribution of emission is isotropic. In that case, (2.9) can be integrated over the direction space, and instead of (2.8) the system to be solved is

$$\begin{aligned} \mathbf{J} &= \mathbf{\Lambda}\bar{\mathbf{j}}_\mathbf{e} \\ \bar{\mathbf{j}}_\mathbf{e} &= \mathbf{f}(\mathbf{J}), \end{aligned} \tag{2.10}$$

where $\mathbf{J}$ and $\bar{\mathbf{j}}_\mathbf{e}$ are $N_{\mathrm{cells}}N_{\mathrm{freq}} \times 1$ matrices and $\mathbf{\Lambda}$ is a $N_{\mathrm{cells}}N_{\mathrm{freq}} \times N_{\mathrm{cells}}N_{\mathrm{freq}}$ matrix.

2.2.2 Solving the linear equation

The problem of numerically evaluating the formal solution, i.e., determining I from equation (2.8) when κ and ϵ are given can be done using several different methods. In the context of molecular clouds, the most commonly used solvers are raytracing algorithms, moment methods, and the Monte Carlo method (Steinacker, 2010; Steinacker et al., 2011).

In raytracing codes the ray direction is discretised into a finite number of bins, and the formal solution (2.2) is integrated for each direction (e.g., Steinacker et al., 2005).

The method is well suited to spectral line calculations (Juvela, 2011). However, in continuum calculations, where anisotropic scattering from dust grains is important, the method is not as efficient. Moment methods are based on a series expansion of the intensity. The methods are very fast in optically thick regions, where the radiation field changes slowly with direction, and only the lowest terms of the series expansion are significant. However, they are not efficient in cases where the radiation intensity changes strongly with direction.

The program described in Paper IV is based on the Monte Carlo method. The Monte Carlo method for radiative transfer can be described intuitively as a simulation of the actual physical processes of radiation transport. The radiation field is simulated by sending photon packages, each of which represents a large number of photons, to the cloud. Photons packages are generated in random locations in the cloud according to the distribution of the emission, and their interactions with the medium are sampled stochastically. For instance, in units of optical thickness, the free path of a photon until its next interaction is exponentially distributed with the mean 1. The track of a photon can be simulated by drawing a random number from an exponential distribution, and moving the photon in a straight line until the optical thickness of the path reaches the sampled value. Then random numbers are used to determine whether the photon is absorbed or scattered, and in the case of scattering, a new direction is chosen stochastically. The probability distributions for different interactions depend on the properties of the medium. The directional distribution is sampled statistically with random numbers, and there is no need to discretise the direction space explicitly.[1] In practice, a Monte Carlo method that is directly analogous to the transport of photons in a cloud is often very inefficient, and various weighting schemes are used improve the speed of the calculation (Juvela, 2005).

The main advantage of the Monte Carlo method is its adaptability. It is easy to include complicated geometries and arbitrary scattering functions. The main drawback is the computational cost of obtaining accurate results. Because of the stochastic nature of the method, the results always contain statistical noise. The noise usually decreases as $1/\sqrt{N}$, when the number of photon packages, N, increases. An acceptable accuracy may require a very large number of packages (in some cases more than billion), and therefore also significant computational resources. However, the fast development of computers has helped to solve the problem. Furthermore, the Monte Carlo method accommodates easy and efficient parallelisation (Robitaille, 2011).

[1] Unless that is needed for the emission calculation.

2.2.3 Iterative solution of the full problem

The full discretised system (2.10) is a non-linear system of equations with, in large models, several million variables. The discretised Λ-operator is then a matrix with more than 10^{12} elements, and constructing and storing the full matrix is usually not possible.

The system of equations (2.8) can be solved without explicitly constructing the Λ-operator by using the Λ-iteration:

$$\begin{array}{rcl} \mathbf{J_{n+1}} & = & \mathbf{\Lambda \bar{j}_n} \\ \mathbf{\bar{j}_{n+1}} & = & \mathbf{f(J_{n+1})}. \end{array} \tag{2.11}$$

Each iteration step entails both solving a linear radiative transfer problem for a given emission coefficient using, e.g., the Monte Carlo method, and calculating the emission coefficient from the radiation field by using the dust model or, in the case of spectral line calculations, by solving the rate equations for the population numbers. In large models both solving the linear radiative transfer equation and calculating the emission coefficient are computationally expensive, limiting the ability to solve the RTE in slowly converging models.

In a model where individual cells are optically thick, most of the radiation emitted in a cell is absorbed in the same cell, and therefore does not contribute to the net energy transfer between different cells. This means that in the matrix representing the Λ-operator the entries on the main diagonal of the matrix are large compared to the other entries, leading to a very slow convergence of the basic Λ-iteration. In the accelerated Λ-iteration the problem of slow convergence is mitigated by explicitly treating the diagonal part of the Λ-operator (Cannon, 1973; Rybicki & Hummer, 1991; Juvela & Padoan, 1999; Hogerheijde & van der Tak, 2000). The operator is written as $\mathbf{\Lambda} = \mathbf{\Lambda_0} + \mathbf{\Lambda_1}$, where $\mathbf{\Lambda_0}$ is a diagonal matrix. The iteration is then run as

$$\begin{array}{rcl} \mathbf{J_{n+1}} & = & \mathbf{\Lambda_0 \bar{j}_{n+1} + \Lambda_1 \bar{j}_n} \\ \mathbf{\bar{j}_{n+1}} & = & f(\mathbf{J_{n+1}}). \end{array} \tag{2.12}$$

Every step of the iteration requires solving a non-linear system of equations. However, because $\mathbf{\Lambda_0}$ is diagonal, the full system decouples into N_{cells} separate systems, each with N_{freq} unknowns. Furthermore, because only the diagonal part of the full Λ operator is needed, storage requirements are much lower. Instead of a diagonal $\mathbf{\Lambda_0}$, a more complex operator that is a better approximation of the full Λ operator can be used. This accelerates convergence, but requires more storage and computation for each step of the iteration (Juvela, 2005).

2.3 Applications of radiative transfer calculations

Perhaps the most obvious use of radiative transfer computations is in the modelling of observations of a specific object, such as a molecular cloud, a circumstellar disc or a dusty spiral galaxy. One can construct a model of the object, run the radiative transfer simulation, and compare the results with the observations. It is also possible to consider the inverse problem of determining the source structure from the observations. For example, an optimisation routine can be used to determine the model parameters that result in the best fit with the observations. Inverse modelling has been applied to targets such as circumstellar structures (Domiciano de Souza et al., 2011), molecular clouds (Steinacker et al., 2005), and dusty galaxies (Hei Law & Gordon, 2012). This is also the approach in Paper I.

The studies focusing on determining the structure of a specific objects with radiative transfer simulations typically use relatively simple models that can be described with only a few parameters. There are two main reasons for this. The first is that there is often a large set of models that can reproduce the observations. To find a unique best solution, the model space needs to be restricted. Another reason is the computational cost of finding the best solution. Solving the RTE even for a single model is time consuming. A family of models described by a large number parameters would need a prohibitive number of evaluations of the radiative transfer model to find the best solution.

Another approach to utilising radiative transfer simulations is to use them as a post-processing step in the study of results from other simulations such as magneto-hydrodynamical (MHD) models of molecular clouds (Goodman, 2011). Even if the MHD simulations do not try to describe any particular astrophysical object, the statistical properties of the models, e.g., the mass distribution of collapsing cloud cores, can be compared to the statistics derived from real observations of a large number of targets. The statistical properties of a model depend on the parameters of the simulation, such as the magnetic field strength, and a comparison with observations can provide insight on the parameter values. Some statistical properties, such as the column density distribution, can be extracted from the model clouds directly without using radiative transfer calculations. However, almost all information from astrophysical objects is obtained through observations of electromagnetic radiation, and it may be difficult to relate the observations to the intrinsic properties of the objects. Radiative transfer computations can be used to construct synthetic observations of model clouds, allowing a direct comparison of real observations and results from simulations. It is possible to simulate observations made with particular telescopes by convolving the intensity map that is obtained from radiative transfer simulation with an appropriate beam shape, and by adding realistic noise to the synthetic map. Paper II and

Paper III follow this approach. On the other hand, radiative transfer calculations can help to determine whether the methods that are used, e.g., in the estimation of the column density from observed dust emission, are accurate. This is the focus of Paper V. Other examples of the use of synthetic observations can be found in Mellema et al. (2006), Krumholz et al. (2007), Commerçon et al. (2012a,b), and Juvela et al. (2012).

Another important application of radiative transfer computations is as an ingredient in radiative-hydrodynamical simulations. For instance, the calculation of the thermal balance and ionisation degree of gas requires solving the RTE for each time step. For this reason the RTE has to be solved very quickly, and usually efficient but relatively low accuracy methods such as the flux-limited diffusion approximation are used (Levermore & Pomraning, 1981). Radiative-hydrodynamical calculations are outside the scope of this thesis, and we refer to books Mihalas & Mihalas (1984) and Castor (2004) for detailed treatments.

Chapter 3

Simulations of dust continuum radiation

In this chapter, we present some applications of dust continuum radiative transfer to the study of ISM. We consider two cases: the thermal emission from the dust grains at far-infrared and sub-millimetre wavelengths (used in Paper V), and the scattering of optical and near-infrared radiation by the dust grains (the subject of Paper I). We briefly discuss how the observations can be used to study the ISM, and how radiative transfer calculations can be used to examine and improve the reliability of the methods.

3.1 Interaction of dust grains with the radiation field

3.1.1 Absorption and scattering

Linear absorption and scattering coefficients κ_a and κ_s in equation (2.4) represent the total absorption and scattering by dust grains per unit length. The absorption coefficient is proportional to the number density of absorbing particles[1], $n_{\rm dust}$, and their efficiency at absorbing radiation that is called the *absorption cross-section* C_a:

$$\kappa_a = n_{\rm dust} C_a. \tag{3.1}$$

As the name suggests, C_a has the units of area. *Scattering cross-section* C_s is defined analogously, and the sum of the absorption and scattering cross-sections, $C_e = C_a + C_s$ is known as the *extinction cross-section*.

Another often used parameter is the (single-scattering) *albedo* a that is defined as

$$a = \frac{C_s}{C_e} = \frac{C_s}{C_a + C_s}. \tag{3.2}$$

It describes what fraction of the radiation a dust grain scatters. If $a = 0$, the dust grain absorbs all the radiation hitting the particle, whereas $a = 1$ implies that no energy

[1] Assuming that the RTE is applicable, see section 2.1.

is absorbed. Absorption and scattering cross-sections (and therefore also albedo) are functions of frequency and the size, shape, and composition of the dust grain.

Scattering kernel K in equation (2.4) is usually called the *scattering phase function*. Often the phase function depends only on the angle $\theta = \arccos(\vec{k} \cdot \vec{k'})$ between the incoming and scattered radiation, that is $K(\vec{k}, \vec{k'}) = \phi(\theta)$. Similar to the absorption and scattering cross sections, the phase function depends on frequency, and on the properties of dust grains.

The *asymmetry parameter* g is a parameter that characterises the shape of the scattering function. It is defined as the average of the cosine of the scattering angle:

$$g = \int_0^\pi \phi(\theta) \cos\theta \, d\cos\theta. \tag{3.3}$$

Thus, asymmetry parameter $g = 1$ means that the phase function is fully forward-throwing, $g = -1$ indicates a fully back-scattering phase function, and values $-1 < g < 1$ means that scattering function is between the extremes. Although the value of g does not define the phase function uniquely, it is often used to describe the scattering functions of dust models. In these cases the phase function is usually taken from a family of functions known as the Henyey–Greenstein phase functions (Henyey & Greenstein, 1941). Within this family the asymmetry parameter determines the phase function uniquely.

Determining the absorption and scattering cross-sections and the scattering phase function as a function of frequency is a difficult problem in electromagnetics. A closed-form solution is possible only in simple cases, such as spherical particles, and usually one has to resort to numerical methods. For detailed descriptions of these computations, see Bohren & Huffman (1983) and Draine & Flatau (1994). In practice, we use the numerically calculated absorption and scattering properties that are available for different dust models.[2]

3.1.2 Emission from the dust grains

Dust grains absorb stellar radiation, which is peaked at the visible wavelengths and re-radiate the energy mainly in the mid- and far-infrared. In the conditions typical of the ISM, large dust grains, i.e., grains with a radius $r \gtrsim 0.05$ μm, are at the equilibrium temperature $T_{\rm dust}$ with the radiation field (see Figs. 4 and 5 in Li & Draine, 2001). According to the Kirchhoff's law, the equilibrium temperature can be calculated by equating the absorbed and emitted energy (Chandrasekhar, 1950)

$$\int_{4\pi}\int_\nu I(\nu, \vec{k}) C_a(\nu) d\nu d\vec{k} = 4\pi \int_\nu B(T_{\rm dust}, \nu) C_a(\nu) d\nu, \tag{3.4}$$

[2]E.g., `http://www.astro.princeton.edu/~draine/dust/dust.html` (accessed 23.9.2012).

where I is the intensity of the radiation field, and B is the Planck function. The temperature depends strongly on the intensity of radiation field. In the solar neighbourhood (but far from individual stars) the typical dust temperature in the diffuse ISM is 16–17 K, while in dense molecular clouds the equilibrium temperature is slightly lower (Planck Collaboration, 2011). The resulting thermal dust emission is obtained from the equation

$$j(\nu) = \kappa(\nu) B(T_{\mathrm{dust}}, \nu). \tag{3.5}$$

Because the dust opacity is a function of the dust composition as well as the grain size, for an accurate calculation the equilibrium temperature and emission must be calculated separately for each dust population (e.g., the silicate and carbonaceous grains), and the grain size distribution must be discretised and each size bin treated separately.

For a small grain, the energy of a photon at ultraviolet or visible wavelengths is sufficient to change the temperature of the grain significantly, in some cases to a temperature of several hundred Kelvin. The absorption of a high energy photon is a rare event, and the grain spends a large fraction of time at a low temperature (Purcell, 1976). Figure 3.1 shows an example of the time-dependent temperature evolution of a very small grain. Although an equilibrium temperature can be calculated from equation (3.4) also in this case, the result calculated from equation (3.5) does not accurately describe the grain emission. Instead of a single dust temperature, the small grains assume a distribution of temperatures that has to be solved to calculate the dust emission accurately (Guhathakurta & Draine, 1989; Siebenmorgen et al., 1992; Draine & Li, 2001). The emission in the mid-infrared is strongly enhanced owing to the fact that the grains occasionally reach high temperatures.

Solving the full temperature distribution is much more computationally demanding than the calculation of the equilibrium temperature, and in large models it is usually not feasible to calculate the distribution directly. Acceleration methods have been developed for the temperature calculations that can decrease computational cost by many orders of magnitude, at the cost of slightly worse accuracy (e.g., Juvela & Padoan, 2003; Baes et al., 2011). Moreover, the effect of the emission from the very small grains is usually insignificant at wavelengths $\lambda > 100$ μm (see Fig. 8 in Li & Draine, 2001), and for the modelling of the far-infrared and sub-millimetre emission, calculating a single equilibrium temperature is often sufficient.

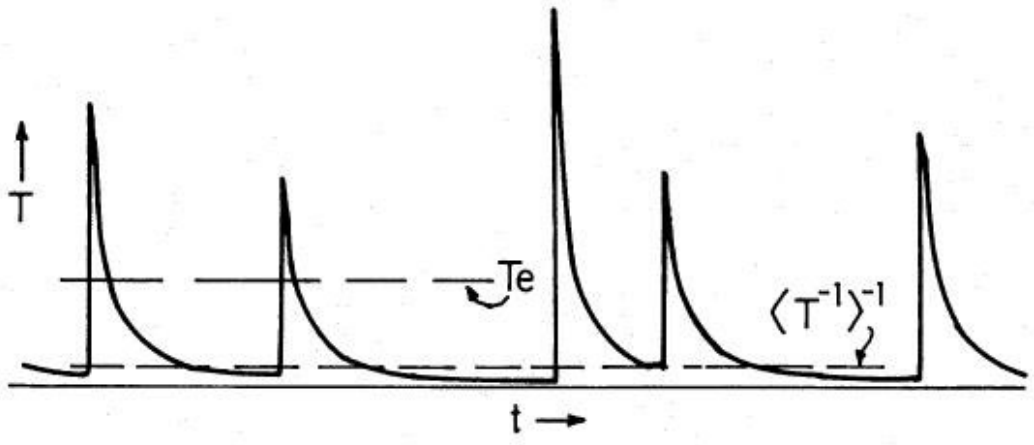

Figure 3.1: Time-dependent temperature of a very small grain in the ISM. Absorption of energetic starlight photons heats the particle to a high temperature. Such absorptions are infrequent events, and in the meantime the grain cools to a very low temperature. T_e indicates the equilibrium temperature of the grain as given by equation (3.4). $\left\langle T^{-1}\right\rangle^{-1}$ is the inverse of the time-average of $1/T$, which is an important quantity in the study of the alignment of dust grains in a magnetic field. From Purcell (1976).

3.2 Applications

3.2.1 Estimating the column density using dust thermal emission

Far-infrared dust emission is commonly used to estimate the mass surface density of molecular clouds. At the far-infrared wavelengths interstellar clouds are generally optically thin ($\tau \ll 1$). If the dust temperature is assumed constant along the line of sight, we get from equation (2.7)

$$I(\lambda) = \tau(\lambda) B(\lambda, T_\mathrm{dust}). \tag{3.6}$$

If we further assume that the dust grain properties do not change along the line of sight, equations (2.3) and (3.1) yield

$$I(\lambda) = \tau(\lambda) B(\lambda, T_\mathrm{dust}) = C_a(\lambda) B(\lambda, T_\mathrm{dust}) \int_\mathrm{LOS} n_\mathrm{dust}(s) ds = C_a(\lambda) B(\lambda, T_\mathrm{dust}) N_\mathrm{dust}. \tag{3.7}$$

Here the integral is taken over the line-of-sight (LOS), and $N_\mathrm{dust} = \int_\mathrm{LOS} n_\mathrm{dust}(s) ds$ is the column density of dust grains.

Generally, T_dust, N_dust, and $C_a(\lambda)$ are all unknown. However, if observations of $I(\lambda)$ are available at m wavelengths and the dust absorption cross section $C_a(\lambda)$ is parametrised as a function of $m-1$ parameters: $C_a(\lambda) = C_a(\lambda_0) f(\lambda/\lambda_0; a_1, \ldots, a_{m-2})$, where λ_0 is a reference wavelength (e.g. 100 μm), it

is possible to solve $T_{\rm dust}$ and the $m-1$ parameters $C_a(\lambda_0)N_{\rm dust}, a_1, \ldots, a_{n-1}$. It can be seen from equation (3.7) that it is only possible to solve for the product of the column density and dust absorption cross section.

At the far-infrared wavelengths, it is usually assumed that $f(\lambda/\lambda_0) = (\lambda/\lambda_0)^{-\beta}$, where β is known as the *spectral index* of the dust (see, e.g., Schwartz, 1982). In that case, observations at three wavelengths are sufficient to determine the dust temperature, the optical thickness of the cloud, and the spectral index. Often a standard value $\beta = 2$ is assumed, in which case observations at only two wavelengths are needed. However, the value of β provides information about the properties of the dust grains, in particular the size distribution, and its determination is of intrinsic interest. If observations are available at more wavelengths than there are free parameters, there are more equations than unknowns, and usually the least-squares solution is sought.

The dust column density can now be found as

$$N_{\rm dust} = \frac{I(\lambda_0)}{C_a(\lambda_0)B(\lambda_0, T_{\rm dust})} \tag{3.8}$$

and the molecular hydrogen column (number) density is

$$N({\rm H_2}) = \frac{N_{\rm dust}}{m_{\rm H} R_{\rm dust} \mu_{\rm H_2}} = \frac{I(\lambda_0)}{C_a(\lambda_0)B(\lambda_0, T_{\rm dust}) m_{\rm H} R_{\rm dust} \mu_{\rm H_2}}, \tag{3.9}$$

where $m_{\rm H}$ is the mass of a hydrogen atom, $R_{\rm dust}$ is the dust-to-gas mass ratio ($\approx 1/100$, see Draine, 2003), and $\mu_{\rm H_2}$ is the mean molecular mass per $\rm H_2$ molecule (2.8 for a gas consisting of 90 % $\rm H_2$ and 10 % He). As noted above, the value of $C_a(\lambda_0)$ cannot be obtained from thermal dust emission observations, and it must be determined using other methods. The column density estimate is inversely proportional to the assumed value of C_a, and its uncertainty can be a significant source of error.

The analysis presented above makes three assumptions about the objects under study. Firstly, it is assumed that the cloud is optically thin at the wavelengths that are used in the estimation of the column density. Although this is often the case, the assumption may be violated in some cores (e.g., Lis & Menten, 1998).

The second assumption is that the dust temperature is constant along the line of sight. This is certainly not the case in interstellar clouds. Although molecular clouds may be optically thin to far-infrared radiation, their optical thickness at visible wavelengths is often significant. The heating radiation field is weaker inside the cloud than in the outer parts, and the dust temperature is not constant (see Bergin & Tafalla, 2007, and references therein). Furthermore, a cloud may contain embedded newly born stars that heat their surroundings.

The third assumption is that the dust properties are constant throughout the cloud. However, this is known not to be true. Observations and theoretical studies indicate that in the cold, dense cores the dust grains acquire ice mantles and may

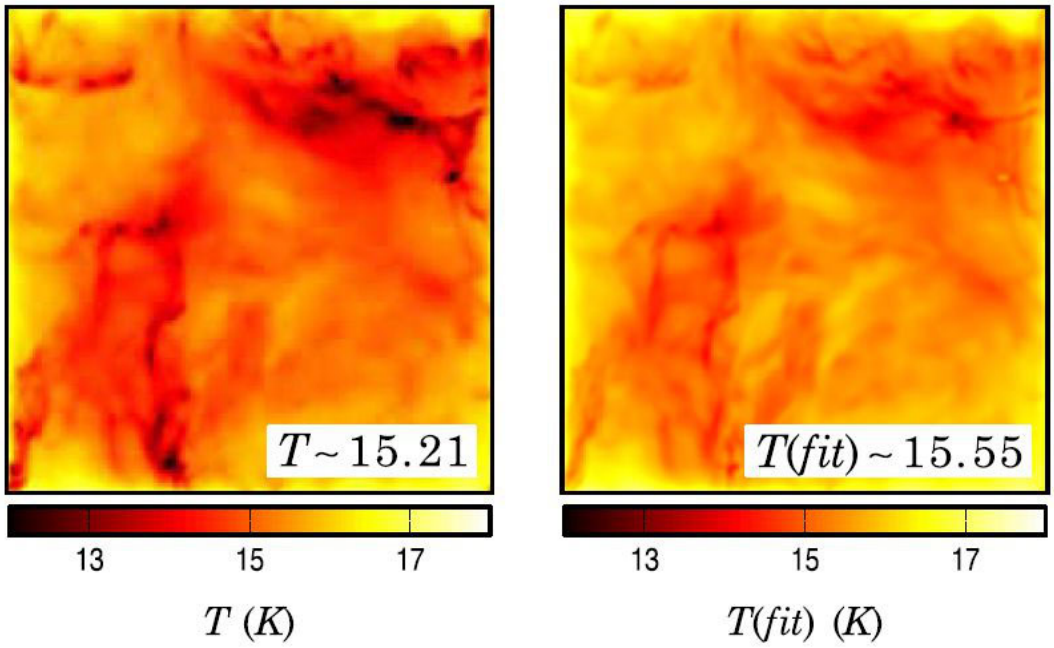

Figure 3.2: A comparison of the true dust temperature and the estimate from far-infrared synthetic observations of a MHD model cloud. The left panel presents a map of the mass-averaged on the line-of-sight, and the right panel shows the temperature determined for simulated 100 μm, 160 μm, 250 μm, 350 μm, and 500 μm observations. The median value of the temperature is written in each frame. See the text for details. Adapted from Paper V.

coagulate to form larger grains (e.g., Ossenkopf, 1993; Ossenkopf & Henning, 1994; Stepnik et al., 2003; Steinacker et al., 2010; Compiègne et al., 2011). This is expected to increase the dust opacity at sub-millimetre wavelengths (i.e., decrease β).

To study whether these factors bias the column density estimates, it is necessary to self-consistently compute the temperature distribution in a realistic model cloud, carry out synthetic observation and analyse them in the same way as real observations. The simulations also help to determine how the intrinsic variation of dust properties is reflected in the observations, and thus provide important input into the dust models. Figure 3.2 shows an example of results from such simulations. The figure shows a comparison of the true temperature that is read directly from the model and the temperature that has been calculated from simulated far-infrared observations. In this case, the difference is significant especially in the upper right parts of the frames where the cloud optical thickness is high. The radiation comes mainly from the warm outer parts of the cloud, while a large amount of cold dust in the dense inner part of the cloud contributes little to the observed surface brightness.

3.2.2 Observations of scattered light

Because the temperature of interstellar dust is typically ∼20 K and even the transiently heated dust grains only reach a maximum temperature of a few hundred Kelvin, thermal emission from the dust grains is negligible at optical and near-infrared wavelengths. Even in circumstellar discs the thermal dust emission is significant at these wavelengths only very close to the star. However, the albedo of the dust grains is relatively high at the visible wavelengths, and they scatter the radiation effectively.

The fact that reflection nebulae are dust clouds that scatter the light from nearby stars was recognised already in the early 20th century (Hubble, 1922). However, even if there are not any stars near a cloud, it scatters the general Galactic radiation, i.e., the combined light from all stars in the galaxy. In this case the surface brightness of the cloud will be lower than in a classical reflection nebula, but it can nevertheless be detected in optical and near-infrared (Lehtinen & Mattila, 1996; Foster & Goodman, 2006), and in some cases also at mid-infrared wavelengths (Steinacker et al., 2010).

Although observations of scattered Galactic light are more difficult because of the low surface brightness compared to a reflection nebula, the interpretation of measurements is easier. In the case where the radiation field is dominated by a nearby source, the exact geometry of the cloud and the locations of the stars illuminating it have a very strong influence on the brightness distribution. In contrast, the strength and the directional distribution of the interstellar radiation field is fairly well known. Furthermore, near a star the dust is warm, and the near-infrared radiation may be partly thermal emission from hot dust grains. At the visible wavelengths a non-thermal emission known as the extended red emission (ERE) has been detected in some reflection nebulae (Witt & Vijh, 2004). ERE is believed to be caused by photoluminescence following absorption of ultraviolet photons.

Observations of scattered Galactic light have been used to study both the structure of interstellar clouds and the properties of the dust grains since the 1930s (Struve & Elvey, 1936; Struve & Story, 1936), and Monte Carlo computations were applied to the problem already in the 1970s (Mattila, 1970; Witt & Stephens, 1974). More recently, the observations have found an application in the mapping of the density structure of molecular clouds. Radiative transfer simulations with realistic cloud models have shown (Juvela et al., 2008, 2009) that the observed surface brightness that is caused by the scattered light is almost directly proportional to the column density, unless the optical thickness of the cloud is high. Figure 3.3 shows the near-infrared surface brightness observed from a filament in the Corona Australis molecular cloud. If $\tau \gtrsim 2$ at the observed wavelength, the surface brightness saturates. Although at the visible wavelengths the method is limited to clouds with a fairly low column density, using near-infrared observations in the K band it is possible to map the column density

reliably in areas with A_V up to 20^{mag}. Compared to other methods that are used for determining the column density, such as the dust emission (see section 3.2.1) or the reddening of background stars (e.g., Lombardi & Alves, 2001), the main advantage is the high, even sub-arcsecond resolution.

In addition to the study of the cloud structure, observations of scattered light can be used to study the scattering properties of dust grains, i.e., their albedo a, and the asymmetry parameter of their scattering phase function g. The parameters are closely related to the composition and size of the scattering grains, and by combining measurements made at several wavelengths dust populations can be studied in detail. Alternatively, it is possible to test whether dust models can reproduce the observations. The study of dust properties is complicated by the fact that the observed surface brightness depends on the unknown three-dimensional structure of the cloud under study. Even in the two-dimensional (a, g) parameter space there is often a degeneracy between a and g, and it is not possible to determine a unique solution. For a review of the study of dust properties using observations of scattered light, see Gordon (2004).

A further application for observations of scattered light is in the study of the interstellar radiation field in different parts of the Milky Way. Surface brightness of the scattered light is proportional to the intensity of the radiation field illuminating the cloud, and if the cloud structure and the properties of dust grains are known, it is possible infer the strength of the radiation field near the cloud. Direct measurements can be used to probe the interstellar radiation field (ISRF) only in the solar neighbourhood, and galaxy models of the distribution of stars and dust have been constructed for calculating the ISRF elsewhere in the Milky Way (e.g. Mattila, 1980; Mathis et al., 1983; Porter & Strong, 2005). Analysis of the Galactic light scattered by a dust cloud can be used to study the ISRF near the cloud, thereby providing a method for validating the results of the Galaxy models.

Figure 3.3: Composite Ks (red), H (green), and J (blue) band image of a part of a filament in Corona Australis molecular cloud. The surface brightness is caused by the scattering of interstellar radiation field by dust grains in the filament. From Juvela et al. (2008).

Chapter 4

Simulations of Zeeman splitting

In this chapter we focus on the role of magnetic fields in the star-formation, and on the use of Zeeman splitting observations in the measurement of magnetic fields in molecular clouds. A more extensive overview of the subject is given in Crutcher (2012).

4.1 Magnetic fields in star-formation

The two competing paradigms for the role of magnetic fields in star-formation make different predictions about some properties of molecular cloud cores, which can, at least in principle, be checked with observations. According to the turbulence-dominated scenario, the duration of the prestellar phase of star-formation is only 1–2 times the free-fall time that can be defined as

$$\tau_{\rm ff} = \frac{3\pi}{32G\bar{\rho}}, \tag{4.1}$$

where $\bar{\rho}$ is the mean density of the core (see Ward-Thompson et al. (2007) for a review). For typical core densities of $n \approx 10^4$ cm^{-3}, $\tau_{\rm ff}$ is approximately 3.5×10^5 years.

In the ambipolar diffusion theory the timescale for core collapse is (Walmsley et al., 2004)

$$\tau_{\rm AD} \approx \frac{2}{\pi G m_n^2} \sum_i \frac{n_i}{n_n} \frac{m_i m_n}{m_i + m_n} < \sigma v >_{in}, \tag{4.2}$$

where m_n is the average mass of neutrals, n_i and n_n are number densities of ions and neutrals, respectively, and the rate coefficient for momentum transfer $< \sigma v >_{in}$ is at low temperatures given by (Flower, 2000)

$$< \sigma v >_{in} = 2\pi e \left(\alpha \frac{m_i + m_n}{m_i m_n} \right)^{1/2}, \tag{4.3}$$

where e is the elementary charge, m_i is the average mass of ions, and α is the polarisability of H_2.

The value of $\tau_{\rm AD}$ varies with the ionisation degree and ionic composition, but for conditions typical of molecular cloud cores $\tau_{\rm AD}/\tau_{\rm ff}$ is several tens to hundreds. The lifetime of cores can be estimated by comparing the number of observed cores and protostars in different stages of evolution, or by studying the time-dependent abundances of chemical species. The results indicate that the core lifetimes are short, $\sim 5 \times 10^5$ years, favouring the turbulence-driven scenario (e.g., Enoch et al., 2008; Pagani et al., 2009; Evans et al., 2009). However, it has been argued that the core lifetimes are strongly underestimated because the cores are only identified in a relatively late stage of collapse (Tassis & Mouschovias, 2004). Furthermore, theoretical calculations and numerical simulations indicate that turbulent fluctuations can decrease the ambipolar diffusion timescale by an order of magnitude (e.g., Kudoh & Basu, 2011).

The two scenarios for star-formation also predict different shapes for the molecular cores. In the turbulence-driven model the magnetic fields are dynamically unimportant, and the shape of the cores is random (Gammie et al., 2003). In contrast, in the ambipolar diffusion scenario the increased support against the gravity in the directions perpendicular to the magnetic field is predicted to result in oblate (flattened ellipsoidal with one axis shorter than the other two) shapes for the cores. Statistical analysis by Tassis et al. (2009) indicates that the oblate ellipsoidal shape is preferred, but the other scenario cannot be ruled out.

The most straightforward method to settling the dispute is to measure the strength of the magnetic field in molecular clouds. The most commonly used parameter describing the importance of the magnetic field is the mass-to-flux ratio, M/Φ, where M is the mass of the core and Φ is the magnetic flux (Crutcher, 1999). It is usually given as a dimensionless normalised value λ that is defined as

$$\lambda = \frac{(M/\Phi)_{\rm obs}}{(M/\Phi)_{\rm crit}}, \tag{4.4}$$

where the critical mass-to-flux ratio is the theoretical value above which the magnetic field cannot support the core (Nakano & Nakamura, 1978). If $\lambda < 1$, the core is called magnetically subcritical, and the magnetic field can counter-balance the self-gravity of the core. If $\lambda > 1$, the core is supercritical, meaning that the magnetic pressure is not enough to stop the collapse.

In practice, instead of the mass and magnetic flux, the mass-to-flux ratio is measured using the column density N (or equivalently, surface density) and the (absolute value of) magnetic flux density, $\|\mathbf{B}\|$. Using the critical mass-to-flux ratio by Nakano & Nakamura (1978), the value of λ can be then determined as

$$\lambda = 7.6 \times 10^{-21} \frac{N({\rm H_2})/1\,{\rm cm^{-2}}}{\|\mathbf{B}\|/1\,\mu{\rm G}}. \tag{4.5}$$

Even measuring λ does not necessarily distinguish between the two paradigms of star-formation. Predictions from both the turbulence-dominated scenario and the

ambipolar diffusion driven process overlap, and mildly supercritical cores ($1 < \lambda \lesssim 3$) are allowed in both models. The issue is further complicated by the fact that, as explained in the following sections, usually only the line-of-sight component of the magnetic field can be determined. The distribution of λ in cloud cores must be inferred statistically from the measured line-of-sight magnetic field strengths. To avoid these complications, more sophisticated measurements have been devised recently to constrain better the role of magnetic fields (Crutcher et al., 2009).

4.2 Observing the magnetic fields

There are five basic methods for the measurement: the Zeeman effect that was studied in Paper II and Paper III and is discussed in more detail in the following sections, the linewidths of spectral lines of ionic and neutral species, the linear polarisation of the thermal emission from dust grains, the linear polarisation of starlight, and the linear polarisation of spectral line emission known as the Goldreich–Kylafis effect.

The difference in linewidths of ionic and neutral species was first proposed as a probe of the magnetic field in Houde et al. (2000a) and Houde et al. (2000b). The magnetic field suppresses the turbulent velocities of the ions, and therefore their spectral lines are narrower than those of the neutrals. However, quantitative estimates are difficult to obtain. The linewidths depend on the abundance variations and excitation conditions in the cores, and careful modelling is needed to interpret the observations. The method requires that the linewidth be dominated by turbulence, and if the linewidth is caused mainly by thermal broadening, no difference between the linewidths of ions and neutrals is expected. However, because in many observations of molecular clouds the linewidths are considerably broader than than the thermal linewidth (e.g., Falgarone & Phillips, 1990), this is not usually a serious limitation.

The linear polarisation of initially unpolarised light from background stars passing through a dust cloud arises from the fact that grains are aligned with their spin axis parallel to the local magnetic field (Davis & Greenstein, 1951). In the case of a non-spherical grain, the long axis of the grain becomes perpendicular to the magnetic field. The exact mechanism that causes the alignment has been debated, see Lazarian (2007) for a review. The grains block most effectively the component of radiation that is polarised parallel to the grain's long axis, i.e., perpendicular to magnetic field. Consequently, the transmitted starlight is polarised parallel to the magnetic field.

The polarisation of far-infrared emission is also caused by the alignment of dust grains. However, because the emission, as well as absorption, is most efficient along the longest axis of the grain, the emitted radiation is polarised perpendicular to the magnetic field. The interpretation of results from the polarisation caused by the dust grain alignment is complicated by the variability of the grain alignment efficiency.

Pelkonen et al. (2007) have shown that because of the low degree of grain alignment in dense cores, the polarised far-infrared dust emission arises mainly from the diffuse regions surrounding the core, and it may not be possible to recover the mass-averaged magnetic field orientation.

The Goldreich–Kylafis effect is the linear polarisation of rotational spectral lines in the presence of a weak magnetic field (Goldreich & Kylafis, 1981, 1982). The effect is strongest for molecules with large permanent electric dipole moments, such as CO. The detailed predictions of the Goldreich–Kylafis effect are model dependent. The orientation of the linear polarisation is either perpendicular or parallel to the projection of the magnetic field, depending on the properties of the velocity field in the object, and the degree of polarisation depends on the anisotropy of the radiation field, and on the gas density. Therefore, it is difficult to determine which parts of the object contribute to the polarised emission and to estimate the true morphology of the magnetic field.

Observations of linear polarisation caused by the alignment dust grains or the Goldreich–Kylafis effect do not provide direct information on the magnetic field strengths. What is obtained is the morphology of the plane-of-sky component of the magnetic field. The dispersion of the measured magnetic field directions can be used to statistically estimate the plane-of-sky magnetic field strength using the Chandrasekhar–Fermi method (Chandrasekhar & Fermi, 1953).

4.3 Zeeman splitting of spectral lines

The Zeeman effect is the splitting of atomic or molecular energy levels in a magnetic field. The splitting results in changes in spectral lines corresponding to the transition between the energy levels, and by analysing the observed spectral lines it is possible to estimate the magnetic field.

The splitting arises from the interaction of the magnetic moment of an atom or a molecule with the external magnetic field. However, only a few atomic or molecular species in the ISM have an appreciable magnetic moment. These are the species with a non-zero net electronic angular momentum or spin resulting from unpaired electrons. Most atoms and molecules of astrophysical interest, such as CO, have no unpaired electrons and thus no net electronic angular momentum or spin. In such a case the magnetic moment results only from the nuclear spin, and is smaller by a factor of more than 10^3.

A very abundant species with a large magnetic moment is the neutral hydrogen. Indeed, the Zeeman splitting in the interstellar matter was first detected in the 21 cm hydrogen line (Verschuur, 1968), and observations of that line have been used extensively in studies of the Galactic magnetic field (see Heiles & Crutcher (2005);

Heiles (2010) and references therein). However, in molecular clouds the abundance of atomic hydrogen is very low, and observations of other tracer species are needed. Besides having a large magnetic moment, a good tracer should be relatively abundant, have suitable (radio frequency) spectral lines, and preferably not vary much in relative abundance throughout the molecular cloud. The most commonly used tracer has been the hydroxyl radical, OH. It is known that OH is strongly depleted at densities $\gtrsim 10^4$ cm^{-3} (van Dishoeck & Blake, 1998) due to freezing onto the dust grains, and therefore it is not useful for studying the densest regions. Observations of the Zeeman splitting in CN lines at 113 GHz have been used to determine the magnetic field in dense cores with 10^4 cm$^{-3} \lesssim n \lesssim 10^6$ cm^{-3} (e.g., Falgarone et al., 2008).

We will briefly review how the Zeeman splitting affects spectral lines. We will focus on the OH 18 cm lines which are a subject of this thesis, although the theory applies largely also to other spectral lines and molecular and atomic species. See Heiles et al. (1993) for a survey of spectral lines, which may be used for Zeeman splitting observations. Figure 4.1 shows the energy level diagram for the OH ground state. The ground state $^2\Pi_{3/2}$ is split due to the interaction between the rotation of the molecule and the orbital motion of the unpaired electron. This effect is known as the Λ-doubling. The Λ-doubling sublevels are further divided into two by the hyperfine splitting owing to interaction of the unpaired electron's spin with the magnetic moment of the hydrogen nucleus. There are four allowed transitions between the levels, at 1612 MHz, 1665 MHz, 1667 MHz, and 1720 MHz (wavelength of ≈ 18 cm). The relative strengths of the spectral lines in thermodynamic equilibrium are 1:5:9:1; the two strongest lines at 1665 MHz and 1667 MHz are known as the main lines, and the 1612 MHz and 1720 MHz are the satellite lines.

In an external magnetic field each of the energy levels is split into $2F+1$ sublevels, where F is the total angular momentum. The magnetic sublevels are denoted by magnetic quantum numbers m_F. Only transitions with $\Delta m_F = 0$ or $\Delta m_F = \pm 1$ are allowed. Transitions with $\Delta m_F = 0$ form the π components of the spectral line, while $\Delta m_F = \pm 1$ transitions cause the $\sigma^{\pm}$ components.

The interaction of atoms and molecules with radiation in a magnetic field is a complex problem and instead of deriving the equations here, we refer to Stenflo (1994) and Trujillo-Bueno et al. (2002) for details. Solving the equations that describe the transfer of polarised radiation and the associated equations for the statistical equilibrium fully self-consistently is a very difficult problem even compared to the scalar radiative transfer equation. The populations of magnetic sublevels have to be calculated separately, taking into account the quantum interferences between the sublevels.

Instead of the full equations, various approximations are often used. In Paper II and Paper III we apply the *field-free* approximation (Rees, 1969), where the pop-

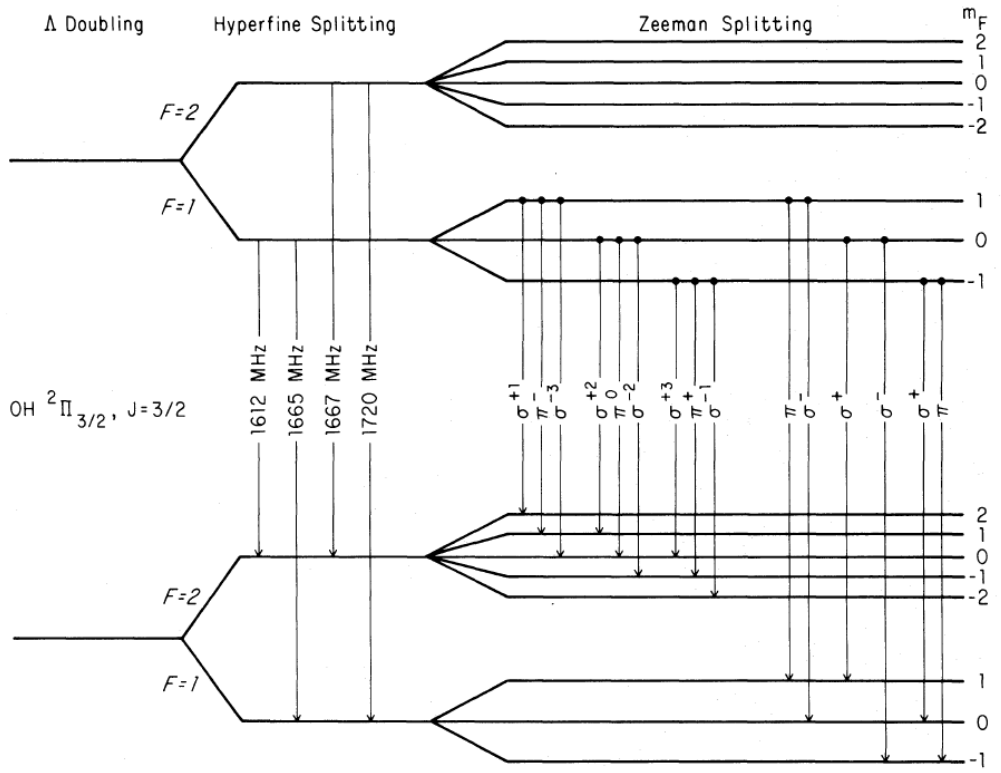

Figure 4.1: Diagram of energy levels in the OH ground state. The state is split into two by the Λ-doubling, and each of the two levels is divided further into two by the hyperfine splitting. In an external magnetic field each of the hyperfine energy levels are split by the Zeeman effect into $2F + 1$ levels. The spacing between these energy levels is proportional to the strength of the magnetic field. Permitted Zeeman transitions at 1612 MHz and 1665 MHz are indicated with arrows. See the text for details. From Hansen (1982).

ulation numbers for the normal (non-magnetic) energy levels are calculated using a scalar radiation transfer code, while the population numbers of the Zeeman sublevels of a single energy level are assumed to be equalised. Under certain further simplifying assumptions, the equations for the Stokes parameters can be written as (Landi Degl'Innocenti, 1976; Rees et al., 1989)

$$\frac{d\mathbf{I}}{ds} = -\mathbf{K}\mathbf{I} + \mathbf{j}, \tag{4.6}$$

where $\mathbf{I} = [I, Q, U, V]^{\mathrm{T}}$ is the column vector of four Stokes components, $\mathbf{K}$ is the 4×4 absorption matrix and $\mathbf{j}$ is the 4×1 emission vector. Matrix $\mathbf{K}$ is given by

$$\mathbf{K} = \kappa_0 \begin{pmatrix} \eta_I & \eta_Q & \eta_U & \eta_V \\ \eta_Q & \eta_Q & \rho_V & -\rho_U \\ \eta_U & -\rho_V & \eta_I & \rho_Q \\ \eta_V & \rho_U & -\rho_Q & \eta_I \end{pmatrix}, \tag{4.7}$$

and $\mathbf{j}$ is

$$\mathbf{j} = \kappa_0 S \begin{pmatrix} \eta_I \\ \eta_Q \\ \eta_U \\ \eta_V \end{pmatrix}, \tag{4.8}$$

where κ_0 is the line centre opacity in the case of no magnetic field and S is the scalar line source function. κ_0 and S are both functions of level populations that are obtained with scalar radiative transfer calculations. Functions $\eta_{I,Q,U,V}$ and $\rho_{Q,U,V}$ are defined as

$$\eta_I = \frac{1}{2}\phi_p \sin^2\gamma + \frac{1}{4}(\phi_r + \phi_b)(1 + \cos^2\gamma), \tag{4.9}$$

$$\eta_Q = \frac{1}{2}[\phi_p - \frac{1}{2}(\phi_r + \phi_b)] \sin^2\gamma \cos 2\chi, \tag{4.10}$$

$$\eta_U = \frac{1}{2}[\phi_p - \frac{1}{2}(\phi_r + \phi_b)] \sin^2\gamma \sin 2\chi, \tag{4.11}$$

$$\eta_V = \frac{1}{2}(\phi_r - \phi_b) \cos\gamma, \tag{4.12}$$

$$\rho_Q = \frac{1}{2}[\xi_p - \frac{1}{2}(\xi_r + \xi_b)] \sin^2\gamma \cos 2\chi, \tag{4.13}$$

$$\rho_U = \frac{1}{2}[\xi_p - \frac{1}{2}(\xi_r + \xi_b)] \sin^2\gamma \sin 2\chi, \tag{4.14}$$

$$\rho_V = \frac{1}{2}(\xi_r - \xi_b) \cos\gamma. \tag{4.15}$$

Here γ is the inclination of the magnetic field to the line of sight, and χ is the azimuthal angle from a fixed axis (see Figure 4.2). Functions $\phi_{b,p,r}$ and $\xi_{b,p,r}$ are the generalised profiles; b and r refer to the blue- and red-shifted σ components, while p is the unshifted π component. In the case of 18 cm OH main lines, the generalised

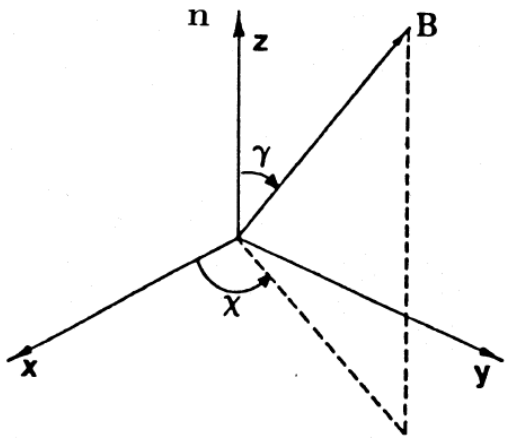

Figure 4.2: The reference frame in which the magnetic field and the Stokes parameters are defined. The z-axis points towards the observer. The angle between the magnetic field **B** and the line-of-sight is denoted with γ, and χ is the azimuthal angle from the x-axis. From Rees et al. (1989).

profiles are given by

$$\phi_p = H(x), \tag{4.16}$$
$$\phi_b = H(x - x_z), \tag{4.17}$$
$$\phi_r = H(x + x_z), \tag{4.18}$$
$$\xi_p = 2F(x), \tag{4.19}$$
$$\xi_b = 2F(x - x_z), \tag{4.20}$$
$$\xi_r = 2F(x + x_z). \tag{4.21}$$

Here $x = (\nu - \nu_0)/\Delta\nu_d$, where ν_0 is the frequency of the transition in the absence of a magnetic field and $\Delta\nu_d$ is the Doppler width of the spectral line, and $x_z = \nu_z/\Delta\nu_d$, where $\nu_z = b\|\mathbf{B}\|$ is the shift caused by the splitting of energy levels in the magnetic field. The value of b depends on the molecular species, and on the transition. For species with a large magnetic moment b is of the order of 1 Hz $\mu\mathrm{G}^{-1}$: in the case of 1665 MHz OH line $b = 1.63$ Hz/μG and for the 1667 MHz line $b = 0.98$ Hz/μG.

Functions H and F are in the general case the Voigt and Faraday–Voigt functions, respectively. In the case of 18 cm OH lines in the ISM, the linewidth is dominated by the Doppler broadening, and we may use the Gaussian profile and the Dawson's function:

$$H(x) = e^{-x^2}, \tag{4.22}$$
$$F(x) = \frac{1}{\sqrt{\pi}} e^{-x^2} \int_0^x e^{-t^2} dt. \tag{4.23}$$

In practice, we use a scalar (non-magnetic) radiative transfer code to determine the population numbers that determine the opacity κ_0 and the line source function S. Then we integrate the system of coupled differential equations (4.6) along the line of sight to calculate the observed Stokes profiles. Figure (4.3) shows an example of simulated 1665 MHz OH Stokes I and V spectra from a MHD model cloud.

4.4 Determining the magnetic field from Zeeman splitting observations

The Zeeman effect results in the spectral line splitting into several (three, in the case of the OH main lines) components in the presence of an external magnetic field. However, in conditions seen in molecular clouds the split in energy levels is very small. The shift is of the order of 1 Hz/μG, so for a typical magnetic field strength of a few tens of μG (Troland & Crutcher, 2008) the split is only ~ 100 Hz, or ~ 20 m s^{-1} in radial velocity units for the 18 cm OH lines. In comparison, the thermal linewidth is usually larger by an order of magnitude, and line broadening due to turbulence often results in a linewidth of more than 1 km s^{-1}. Therefore, it is usually not possible to observe separate Zeeman components. The exception to this are OH and H_2O masers (e.g., Reid & Silverstein, 1990; Surcis et al., 2011). In masing regions the magnetic fields can be strong, of the order of a few mG, and the spectral lines can be much narrower than the thermal linewidth. In these cases the individual Zeeman components can sometimes be seen, and the total magnetic field strength can be determined directly from the separation of the components. However, maser lines probe very localised (possibly shock compressed) regions that may not be representative of the conditions in normal molecular cloud cores.

In other cases it is still possible to determine the line-of-sight component of the magnetic field using the polarisation of spectral lines, in particular the circular polarisation. The Stokes V spectrum emitted in a magnetic field can be written using equations (4.12), and (4.16)–(4.17) as

$$\eta_V(x) = \kappa_0 S \frac{1}{2}(\phi_r(x) - \phi_b(x)) \cos\gamma = \kappa_0 S \frac{1}{2}\left[H(x + x_z) - H(x - x_z)\right] \cos\gamma. \quad (4.24)$$

When $x_z \ll 1$, which is usually the case in molecular clouds, we can approximate $H(x + x_z) - H(x - x_z) \approx 2x_z H'(x)$ and get

$$\eta_V(x) \approx \kappa_0 S \frac{dH(x)}{dx} x_z \cos\gamma. \quad (4.25)$$

On the other hand, when x_z is small, (4.9) and (4.16)–(4.18) yield

$$\eta_I(x) \approx \kappa_0 S H(x). \quad (4.26)$$

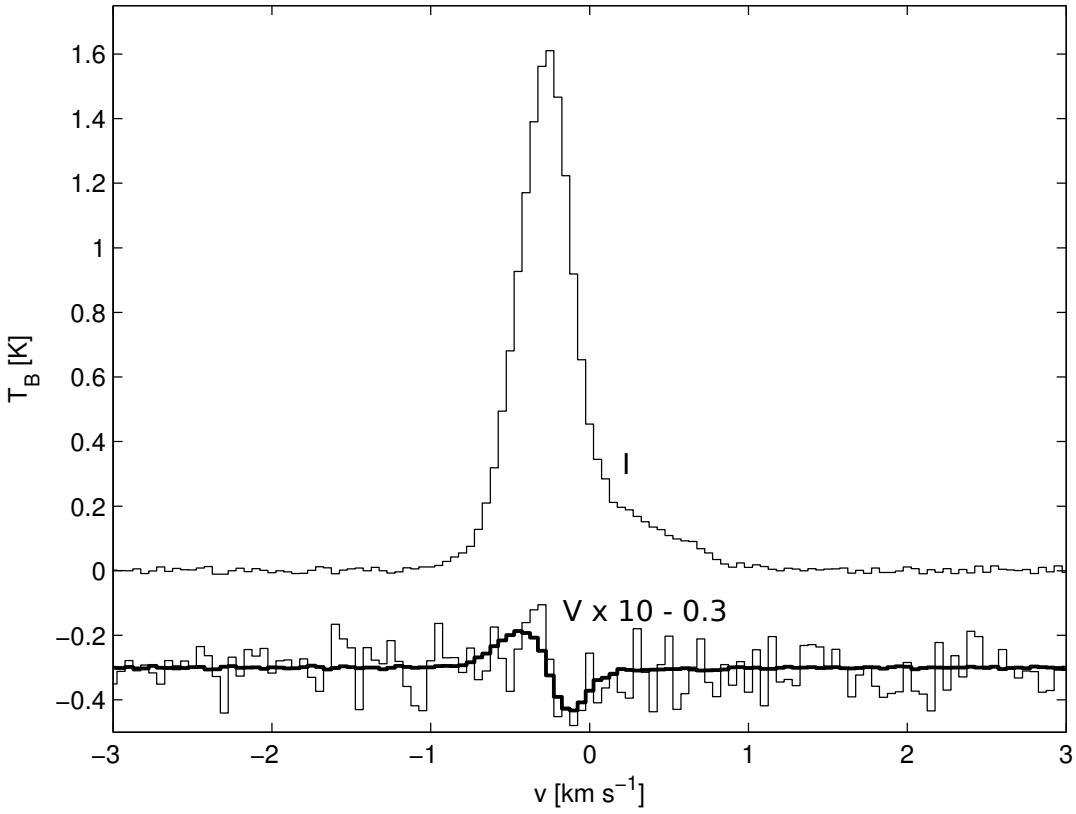

Figure 4.3: An example of simulated Stokes I and V spectra of the 1665 MHz OH line from a core in a MHD cloud model. The Stokes V spectrum has been scaled up by a factor of 10 and offset from zero by 0.3 K for clarity. Gaussian noise at a level similar to recent OH Zeeman surveys (e.g., Bourke et al., 2001; Troland & Crutcher, 2008) has been added to the spectra. The bold line shows the fitted derivative $dI/d\nu$ corresponding to the best-fit line-of-sight magnetic field strength of $B_{\rm LOS} \approx 10.4$ μG. The fitted derivative of the I spectrum follows closely the Stokes V signal with no signs of components with different magnetic fields. However, even in this case the signal-to-noise ratio of the Stokes V signal is relatively poor. The spectra are from simulations that are discussed in Paper III.

If we further assume that the line is optically thin, the excitation temperature is constant along the line of sight, there are no velocity gradients, and the magnetic field strength and direction is constant along the line of sight, using (2.7) we obtain

$$I(x) \approx \tau S H(x), \tag{4.27}$$

$$V(x) \approx \tau S x_z \cos\gamma \frac{dH(x)}{dx}, \tag{4.28}$$

whence

$$V(x) \approx \frac{dI(x)}{dx} x_z \cos\gamma. \tag{4.29}$$

Thus, the observed Stokes V spectrum is a scaled copy of the derivative of the Stokes I spectrum. Because $x_z = b\mathbf{B}/\Delta\nu_d$, we can solve the strength and direction (towards or away from the observer) of the line-of-sight magnetic field, $B_{\mathrm{LOS}} \equiv \cos\gamma\|\mathbf{B}\|$, using the known Zeeman splitting parameter b for the transition. In practice, this is usually done by least-squares fitting a scaled copy of the derivative of the I spectrum to the V spectrum (see Sault et al., 1990, for details).

Observations of the Zeeman splitting in molecular cloud cores are technically very demanding. At the typical magnetic field strengths of a few tens of μG, the brightness temperature of the Stokes V signal is of the order of a few tens of mK. To obtain a robust detection, an integration time of ten hours or more for each pointing is needed even with the largest radio telescopes. As a result, the total number of statistically significant detections in OH Zeeman surveys (Crutcher et al., 1993; Crutcher, 1999; Bourke et al., 2001; Troland & Crutcher, 2008) is only a few dozen. Furthermore, one must be careful to eliminate various observational effects that may lead to spurious detections. In particular, the "beam squint" (Crutcher et al., 1993), meaning that the two orthogonal polarisations have different pointing centres on the sky, can mimic the Zeeman splitting signal.

Although it is not possible to determine the plane-of-sky magnetic field using the Stokes I and V spectra, similar calculations as above show that $Q(x) \propto (\cos\chi - \sin\chi)(x_z \sin\gamma)^2$ and $U(x) \propto \sin\chi(x_z \sin\gamma)^2$. Therefore, observations of all four Stokes parameters would be enough to determine the strength and orientation of the magnetic field completely. However, because the Stokes Q and U signals are proportional to x_z^2 and $x_z \ll 1$, the linear polarised components are weaker than the Stokes V spectrum by at least an order of magnitude. As a result, observing the linear polarisation of spectral lines caused by the Zeeman splitting is currently not possible. Because only one component of the magnetic field can be determined, Zeeman splitting measurements do not allow estimating key parameters such as the mass-to-flux ratio for individual objects. However, if observations of a large number of clouds are available, the true distribution of the magnetic field strength can be inferred with statistical methods (Crutcher et al., 2010).

The method described above is commonly used to derive the line-of-sight magnetic field strengths in molecular clouds. However, for real clouds many of the assumptions made in the analysis do not hold. For instance, the magnetic field morphology along the line of sight, and within the telescope beam may be very complex. Furthermore, the gas density and the excitation temperature of OH molecules are not constant, and it is not clear how much influence different parts of the cloud have on the observed Stokes spectrum. These factors make it difficult to assess whether the predictions from different models agree with the Zeeman splitting observations of molecular cloud cores. To study these questions, it is necessary to use radiative transfer simulations with realistic cloud models.

Chapter 5

Summary of the publications

The thesis consists of five journal publications:

- **Paper I:** T. Lunttila and M. Juvela, 2007, "Inferring the dust properties and density distribution in the outer envelope of IRC +10 216 from scattered Galactic light", Astron. & Astrophys., 470, 259
- **Paper II:** T. Lunttila, P. Padoan, M. Juvela, and Å. Nordlund, 2008, "The Super-Alfvénic Model of Molecular Clouds: Predictions for Zeeman Splitting Measurements", Astrophys. Journal Letters, 686, 91
- **Paper III:** T. Lunttila, P. Padoan, M. Juvela, and Å. Nordlund, 2009, "The Super-Alfvénic Model of Molecular Clouds: Predictions for Mass-to-Flux and Turbulent-to-Magnetic Energy Ratios", Astrophys. Journal Letters, 702, 37
- **Paper IV:** T. Lunttila and M. Juvela, 2012, "Radiative transfer on hierarchial grids", Astron. & Astrophys., 544, A52
- **Paper V:** J. Malinen, M. Juvela, D. C. Collins, T. Lunttila, and P. Padoan, 2011, "Accuracy of core mass estimates in simulated observations of dust emission", Astron. & Astrophys., 530, A101

The papers are summarised below. The author's contribution to the papers is described at the end of each section.

5.1 Paper I

Paper I focuses on the study of light scattering in the dust envelope surrounding the carbon star IRC +10 216. Intermediate mass stars lose a large fraction of their initial mass in their asymptotic giant branch (AGB) phase. The lost mass forms a dust cocoon around the star. As AGB carbon stars are believed to be the major source of

carbonaceous interstellar dust, the study of their envelopes can be used for improving models of newly formed dust.

In the article radiative transfer calculations are used to study the dust properties and the density distribution in the envelope surrounding IRC +10 216. The results are compared to observations reported in the literature by Mauron et al. (2003) and Leão et al. (2006). IRC +10 216 is the closest AGB carbon star to the Sun, and it has been studied extensively. However, different studies have found somewhat conflicting dust properties (e.g., Bagnulo et al., 1995; Skinner et al., 1998).

The article focuses on the modelling of the interstellar radiation that has been scattered by the envelope (emission from the dust grains is negligible at the wavelengths considered in the paper). Compared to modelling the transport of light from the central star, this has some advantages. In particular, the complex and largely unknown structure of the inner envelope is not important when only the scattering of the interstellar radiation is considered. Furthermore, the simulations can be used to study the strength of the interstellar radiation field near the cloud.

The scattered flux is calculated in U, B, and V bands. We use several spherically symmetric envelope models, corresponding to different mass-loss histories. The dust mixture consists of spherical amorphous carbon and silicon carbide grains. Simulations are run with several grain sizes. A key difference to earlier studies of light scattering in the envelope surrounding IRC +10 216 is the use of a realistic ISRF model. The strength of the ISRF varies by a factor of 5–10 depending on viewing direction, with much higher intensity towards low galactic latitudes than towards the galactic poles (Mattila, 1980). At the visible wavelengths the scattering phase function of the dust grains is strongly forward throwing, and the directional distribution of the radiation field impinging on the dust envelope is very important.

The simulations show that the dominant grain size in the envelope must be relatively large, $a \gtrsim 0.1$ μm. With small grains the shape chromatism, i.e., the change of the envelope brightness profile with wavelength, is much stronger than what is observed. Steepness of the brightness profile shows that the mass-loss rate has increased with time, with an approximately 20–50 % increase in 1000 years. The brightness of the envelope is found to be unexpectedly low. The simulations predict a surface brightness higher by a factor of $\sim$2 when an external radiation field given by Galaxy models is used together with the grain properties and density distribution that provide the best fit for the shape of the brightness profile.

The author ran the radiative transfer calculations and wrote the article. The radiative transfer code that was used in the simulations is written by M. Juvela with some modifications contributed by the author. M. Juvela also provided comments and suggestions during the writing of the paper.

5.2 Paper II

As explained in Section 1.3, the role of magnetic fields in star-formation is currently a hotly debated subject. A new method developed by R. Crutcher aims to answer the question about the importance of the magnetic field support for cloud cores. Crutcher et al. (2009) describe a set of measurements that can discriminate between the turbulence-driven and the basic ambipolar diffusion model of star-formation. In brief, the method consists of measuring the *relative mass-to-flux ratio*, $\mathcal{R}_\mu$, which is defined as the ratio of the mass-to-flux ratios in the centre of the core and its envelope:

$$\mathcal{R}_\mu = \frac{[N(\mathrm{H_2})/B_{\mathrm{LOS}}]_{\mathrm{core}}}{[N(\mathrm{H_2})/B_{\mathrm{LOS}}]_{\mathrm{envelope}}} = \frac{[N(\mathrm{OH})/B_{\mathrm{LOS}}]_{\mathrm{core}}}{[N(\mathrm{OH})/B_{\mathrm{LOS}}]_{\mathrm{envelope}}}, \tag{5.1}$$

where $N(\mathrm{H_2})$ is the column density of molecular hydrogen and B_{LOS} is the strength (flux density) of the line-of-sight component of the magnetic field. In practice, the measurement is done by observing at five positions: the centre of the core and four positions in the envelope located symmetrically around the centre.

The test avoids some of the problems faced by the direct measurement of the mass-to-flux ratio in the cores. For instance, it is not necessary to know the relative abundance of the tracer molecule, or the orientation of the magnetic field, although it is assumed that the relative abundance and the field direction do not change from the core centre to its envelope. Furthermore, because the observed normalised mass-to-flux ratios of $\lambda \approx 2$ (see equation 4.5 and the discussion following it) are compatible with both the ambipolar diffusion and the turbulence-dominated scenario, other tests are needed to distinguish between the models.

The relative mass-to-flux ratio provides a direct test of the ambipolar drift model, which requires $\mathcal{R}_\mu > 1$ (Ciolek & Mouschovias, 1994). In the case of a super-Alfvénic model determining the distribution of $\mathcal{R}_\mu$ is more difficult than in the case of the ambipolar diffusion because of the very complicated morphology of the magnetic fields. The magnitude and direction of the field changes along the line of sight, and within the telescope beam. In this article we use radiative transfer calculations to obtain synthetic observations of a super-Alfvénic MHD cloud model.

We select a total of 139 molecular cloud cores from simulated ^{13}CO maps, and calculate the Stokes I and V spectra of the OH 1665 MHz and 1667 MHz lines from the cores. The spectra are calculated using the same beam set-up as in the observations. The line-of-sight magnetic field and the column density are determined from the spectra in the same way as in the observations by Crutcher et al. (2009).

We find a significant scatter in $\mathcal{R}_\mu$. However, for most cores $\mathcal{R}_\mu < 1$, opposite of what the ambipolar diffusion dominated model predicts. We also find some cases where the line-of-sight component of the magnetic field has a different sign in two beams. This behaviour is not predicted by the ambipolar diffusion model. The results

from our simulations agree with the observational results by Crutcher et al. (2009), and thus the turbulence driven scenario of star-formation seems to be favoured over the basic ambipolar diffusion model. However, one should be cautious in interpreting the results. The measurements are technically very demanding and time-consuming, and especially determining the field strength in the core envelope, where the column density is lower, is difficult. Crutcher et al. (2009) were only able to measure $\mathcal{R}_\mu$ in four cores, and even in these cases the uncertainties of the field strengths are significant. Furthermore, the assumption of constant relative OH abundance in the core and the envelope may not be accurate.

The author wrote the radiative transfer program that was used for the calculations, ran the radiative transfer simulations, and analysed the results. The author wrote sections 3 and 4, and together with P. Padoan sections 1 and 5. P. Padoan provided the MHD snapshots and wrote section 2.

5.3 Paper III

Paper III continues with the same theme as Paper II: the simulation of OH Zeeman splitting observations from a super-Alfvénic MHD model cloud. In this article we focus on the mass-to-flux ratio measurements, i.e., determining $N(\mathrm{H_2})/B_{\mathrm{LOS}}$. Although the measured mass-to-flux ratio for a single cloud cannot be used to determine the role of the magnetic field support in any individual cloud because of the unknown alignment of the field, by observing a large number of cores it is possible to statistically infer the distribution of the total magnetic field strength.

In this paper we aim to use synthetic observations of a super-Alfvénic model cloud to simulate OH Zeeman splitting measurements reported in the literature (e.g., Crutcher, 1999; Bourke et al., 2001; Troland & Crutcher, 2008) as closely as possible. The cores are selected from ^{13}CO maps, and noise at a level similar to recent OH Zeeman surveys is added to the synthetic observations. The synthetic observations are made at three assumed cloud distances, and the results are compared to OH Zeeman splitting measurements reported in the literature.

We find that the line-of-sight magnetic field determined from the OH Zeeman splitting strongly overestimates the true mean line-of-sight field strength. This results from the fact that the OH emission comes mostly from the densest cores, where also the magnetic field is strongest. Thus, a strong mean magnetic field is not required to explain the observed line-of-sight magnetic fields.

The distribution of the key parameters such as the mass-to-flux ratio and the turbulent-to-magnetic energy ratio in the synthetic observation is similar to what has been found in OH Zeeman splitting observations by Troland & Crutcher (2008). We conclude that the super-Alfvénic turbulence model of star-formation is consistent with

the OH Zeeman splitting observations.

The author wrote the radiative transfer program that was used for the Zeeman splitting calculations, ran the radiative transfer simulations, and analysed the results. The author wrote sections 3 and 4. Sections 1 and 5 were written jointly with P. Padoan, who also provided the MHD snapshots and wrote section 2.

5.4 Paper IV

As discussed in Section 2 of this thesis, solving the radiative transfer equation is numerically a very difficult problem. For a realistic representation of inhomogenous structures such as turbulent molecular clouds, a three dimensional model is needed. An accurate description of the structure often requires the inclusion of a large variety of scales. For instance, a model of a circumstellar disc may require a resolution of the order of a Solar radius near the star, while, to include the whole disc, the total extent of the model needs to be several hundred AU. On a uniform cartesian grid such a model would comprise hundreds of billions cells. To reduce computational cost, several 3D radiative transfer codes (see the references in section 2.3) have been developed with support for adaptive resolution, i.e., the possibility of using a higher resolution in some parts of the model. With adaptive resolution it is possible to use the finest resolution only where necessary, thereby reducing the number of cells in the model, in some cases by many orders of magnitude.

This article presents new algorithms for efficient dust continuum radiative transfer using adaptive resolution. We present improvements to both the solution of the linear problem, and the iterative process that is needed to calculate the dust temperature in cases where the dust self-coupling is important. The program described in the article uses a hierarchical system of nested grids. The linear problem is solved using the Monte Carlo method. The program works grid-by-grid, moving to the next only after all photon packages in a grid have been processed, instead of following one photon package at a time through the whole model. This provides some computational advantages, e.g., more efficient cache usage.

For the iterative process an important new feature is the possibility of using sub-iterations, i.e., iterating separately those parts of the model that suffer from slow convergence. For instance, in a model of a molecular cloud only a small number of dense cores may need a large number of iterations. The use of sub-iterations allows iterating the cores separately, potentially reducing the computational cost by more than an order of magnitude.

We describe the new algorithms in detail, and examine their efficiency and accuracy in two models. In the case of the first model, a molecular cloud from a MHD simulation, we compare the speed and accuracy of the solution algorithm for the lin-

ear problem in a full resolution model to an adaptive model with a much smaller number of cells. We find that computations with the adaptive model are faster by a factor of several, while the relative root-mean-square (RMS) difference between the surface brightness calculated with the full resolution and the adaptive models is less than 4 % at all wavelengths. In dense cores, where the adaptive grid has the finest resolution, the relative difference is $\lesssim 10^{-4}$. In the second model, a circumstellar disc with a very high optical depth, we focus on the use of sub-iterations. We find that the sub-iteration algorithm is in the test case faster by a factor of two, but in other models the gain can be much larger.

The radiative transfer program is based on a code by M. Juvela. The author has developed the algorithms described in the paper, and added them to the existing program. The author was responsible for writing the paper with assistance from M. Juvela, and for running the simulations.

5.5 Paper V

Observations of thermal dust emission at infrared and sub-millimetre wavelengths are commonly used to determine the masses of molecular cloud cores. However, the estimates may be biased because of dust temperature differences along the line of sight, or the variation of dust grain properties in the dense cores. In this article we use synthetic observations to determine the reliability of the mass estimates in different scenarios. We also study whether the intrinsic dust properties, in particular the spectral index β, can be robustly inferred from the observations.

We use three MHD models representing clouds in different stages of collapse. The models of the most advanced stages of collapse use adaptive grids to resolve the small, dense cores. In some of the simulations we include newly formed stars embedded in the cores to study how the mass estimates are biased by strong temperature gradients.

We use radiative transfer simulations to calculate surface brightness maps at five wavelengths corresponding to the bandpass of the PACS and SPIRE instruments of the Herschel satellite (Pilbratt et al., 2010). Noise typical of Herschel observations is added to the maps, and the maps are convolved to the resolution of the Herschel instruments. The masses are estimated by first solving the colour temperature from the observed surface brightness at different wavelengths, and then solving the column density using the calculated dust (colour) temperature and the known dust opacity, as explained in section 3.2.1. The results are compared to the true values that are obtained directly from the cloud model.

We find that the shape of the core mass spectrum is fairly robust against biases arising from the spatial variations in dust properties or radiative transfer effects. However, the inferred absolute masses of the cores may differ strongly from the true

values. For cores with a very high optical thickness and no embedded star, the error can be a factor of several. In cores that contain a heating source, the errors are typically much smaller. We find that the estimates for the dust spectral index β are strongly influenced by the temperature variations along the line of sight.

The author wrote together with M. Juvela the radiative transfer program that was used for the calculations (the program described in Paper IV), ran a part of the radiative transfer simulations, wrote section 2.2. with M. Juvela, and provided suggestions and corrections during the writing of the other parts of the paper.

Chapter 6

Conclusions and future prospects

Radiative transfer modelling is an indispensable ingredient in the study of the ISM. Without a good understanding of how the observed radiation is created and how it is modified by scattering and absorption, it is impossible to obtain detailed information about the structure of molecular clouds, and the physical conditions in them. Radiative transfer simulations are also vitally needed for relating the predictions resulting from numerical simulations of astrophysical objects, such as MHD models of molecular clouds, to observations.

Four of the five articles in this thesis present examples of the use of radiative transfer calculations. Apart from the articles included in the thesis, we have applied radiative transfer simulations to the analysis of Herschel observations of cold cores (Juvela et al., 2011), and the study of filamentary structures in molecular clouds (Juvela et al., 2012). The radiative transfer code that is described in Paper IV was used in both cases. As a new application, we are currently using radiative transfer calculations to produce synthetic far-infrared observations of the Antennae galaxies (Karl et al., in prep.). The model of the merging galaxies is based on a detailed N-body/hydrodynamical simulation (Karl et al., 2010).

The rapid development of computing capabilities has allowed the use of increasingly detailed models. However, during the last few years the processing speed of a single computing core has been improving only slowly. For instance, the CPU clock rate has remained at 3–4 GHz for almost ten years.[1] Most of the performance increase is from a larger degree of parallelism. It is crucial that new algorithms be developed to take advantage of massively parallel supercomputers and emerging computing paradigms such as stream processing using graphics processing units.

New observations present increasing challenges to the radiative transfer simulations. The very-high-angular-resolution data produced by existing and planned observatories such as the ALMA interferometer (Wootten & Thompson, 2009) and the

[1] However, there has been some improvement in the single-thread performance due to other factors such as larger caches.

next-generation optical and infra-red telescopes – including, for instance, the European Extremely Large Telescope (Gilmozzi & Spyromilio, 2007) and the James Webb Space Telescope (Gardner et al., 2006) – require new modelling tools that can be used to study small, optically thick structures such as circumstellar discs. In addition to the higher resolution, radiative transfer models need to be improved by including more realistic descriptions of physical processes, for example improved dust models. Further challenges await in the integration of realistic radiative transfer simulations with MHD calculations and chemistry modelling into a fully self-consistent simulation the star-formation process.

Bibliography

Acreman, D. M., Harries, T. J., & Rundle, D. A. 2010, Monthly Notices of the Royal Astronomical Society, 403, 1143

André, P., Basu, S., & Inutsuka, S. 2009, in Structure Formation in Astrophysics, ed. G. Chabrier (Cambridge University Press), 254

Arzoumanian, D., André, P., Didelon, P., et al. 2011, Astronomy & Astrophysics, 529, L6

Baes, M., Verstappen, J., De Looze, I., et al. 2011, The Astrophysical Journal Supplement Series, 196, 22

Bagnulo, S., Doyle, J. G., & Griffin, I. P. 1995, Astronomy & Astrophysics, 301, 501

Ballesteros-Paredes, J., Klessen, R. S., Mac Low, M.-M., & Vazquez-Semadeni, E. 2007, Protostars and Planets V, 63

Bergin, E. A., & Tafalla, M. 2007, Annual Review of Astronomy & Astrophysics, 45, 339

Bohlin, R. C. 1975, The Astrophysical Journal, 200, 402

Bohlin, R. C., Savage, B. D., & Drake, J. F. 1978, The Astrophysical Journal, 224, 132

Bohren, C. F., & Huffman, D. R. 1983, Absorption and scattering of light by small particles (Wiley)

Bourke, T. L., Myers, P. C., Robinson, G., & Hyland, A. R. 2001, ApJ, 554, 916

Cannon, C. J. 1973, The Astrophysical Journal, 185, 621

—. 1985, The Transfer of Spectral Line Radiation (Cambridge University Press)

Castor, J. I. 2004, Radiation Hydrodynamics (Cambridge University Press)

Chandrasekhar, S. 1950, Radiative transfer (Clarendon Press)

Chandrasekhar, S., & Fermi, E. 1953, The Astrophysical Journal, 118, 113

Ciolek, G. E., & Mouschovias, T. C. 1994, The Astrophysical Journal, 425, 142

Commerçon, B., Launhardt, R., Dullemond, C., & Henning, T. 2012a, Astronomy & Astrophysics, 545, A98

Commerçon, B., Levrier, F., Maury, A. J., Henning, T., & Launhardt, R. 2012b, ArXiv e-prints:1210.1023

Compiègne, M., Verstraete, L., Jones, A., et al. 2011, Astronomy & Astrophysics, 525, A103

Crutcher, R. M. 1999, The Astrophysical Journal, 520, 706

—. 2012, Annual Review of Astronomy & Astrophysics, 50, 29

Crutcher, R. M., Hakobian, N., & Troland, T. H. 2009, The Astrophysical Journal, 692, 844

—. 2010, Monthly Notices of the Royal Astronomical Society, 402, L64

Crutcher, R. M., Troland, T. H., Goodman, A. A., et al. 1993, The Astrophysical Journal, 407, 175

Davis, Jr., L., & Greenstein, J. L. 1951, The Astrophysical Journal, 114, 206

Domiciano de Souza, A., Bendjoya, P., Niccolini, G., et al. 2011, Astronomy & Astrophysics, 525, A22

Doty, S. D., & Neufeld, D. A. 1997, The Astrophysical Journal, 489, 122

Draine, B. T. 2003, Annual Review of Astronomy & Astrophysics, 41, 241

Draine, B. T., & Flatau, P. J. 1994, Journal of the Optical Society of America A, 11, 1491

Draine, B. T., & Li, A. 2001, The Astrophysical Journal, 551, 807

—. 2007, The Astrophysical Journal, 657, 810

Enoch, M. L., Evans, II, N. J., Sargent, A. I., et al. 2008, The Astrophysical Journal, 684, 1240

Evans, II, N. J., Dunham, M. M., Jørgensen, J. K., et al. 2009, The Astrophysical Journal Supplement Series, 181, 321

Falgarone, E., & Phillips, T. G. 1990, The Astrophysical Journal, 359, 344

Falgarone, E., Troland, T. H., Crutcher, R. M., & Paubert, G. 2008, Astronomy & Astrophysics, 487, 247

Fiedler, R. A., & Mouschovias, T. C. 1992, The Astrophysical Journal, 391, 199

—. 1993, The Astrophysical Journal, 415, 680

Flower, D. R. 2000, Monthly Notices of the Royal Astronomical Society, 313, L19

Foster, J. B., & Goodman, A. A. 2006, The Astrophysical Journal Letters, 636, L105

Gammie, C. F., Lin, Y.-T., Stone, J. M., & Ostriker, E. C. 2003, The Astrophysical Journal, 592, 203

Gardner, J., Mather, J., Clampin, M., et al. 2006, Space Science Reviews, 123, 485, 10.1007/s11214-006-8315-7

Gilmozzi, R., & Spyromilio, J. 2007, The Messenger, 127, 11

Goldreich, P., & Kylafis, N. D. 1981, The Astrophysical Journal Letters, 243, L75

—. 1982, The Astrophysical Journal, 253, 606

Goodman, A. A. 2011, in IAU Symposium, Vol. 270, Computational Star Formation, ed. J. Alves, B. G. Elmegreen, J. M. Girart, & V. Trimble, 511–519

Gordon, K. D. 2004, in Astronomical Society of the Pacific Conference Series, Vol. 309, Astrophysics of Dust, ed. A. N. Witt, G. C. Clayton, & B. T. Draine, 77

Guhathakurta, P., & Draine, B. T. 1989, The Astrophysical Journal, 345, 230

Hansen, S. S. 1982, The Astrophysical Journal, 260, 599

Harju, J., Juvela, M., Schlemmer, S., et al. 2008, Astronomy & Astrophysics, 482, 535

Hei Law, K., & Gordon, K. D. 2012, in American Astronomical Society Meeting Abstracts, Vol. 219, American Astronomical Society Meeting Abstracts, #343.12

Heiles, C. 2010, Highlights of Astronomy, 15, 428

Heiles, C., & Crutcher, R. 2005, in Lecture Notes in Physics, Berlin Springer Verlag, Vol. 664, Cosmic Magnetic Fields, ed. R. Wielebinski & R. Beck, 137

Heiles, C., Goodman, A. A., McKee, C. F., & Zweibel, E. G. 1993, in Protostars and Planets III, ed. E. H. Levy & J. I. Lunine, 279–326

Henyey, L. G., & Greenstein, J. L. 1941, The Astrophysical Journal, 93, 70

Hogerheijde, M. R., & van der Tak, F. F. S. 2000, Astronomy & Astrophysics, 362, 697

Hollenbach, D., & Salpeter, E. E. 1971, The Astrophysical Journal, 163, 155

Houde, M., Bastien, P., Peng, R., Phillips, T. G., & Yoshida, H. 2000a, The Astrophysical Journal, 536, 857

Houde, M., Peng, R., Phillips, T. G., Bastien, P., & Yoshida, H. 2000b, The Astrophysical Journal, 537, 245

Hubble, E. P. 1922, The Astrophysical Journal, 56, 400

Jonsson, P. 2006, Monthly Notices of the Royal Astronomical Society, 372, 2

Juvela, M. 2005, Astronomy & Astrophysics, 440, 531

Juvela, M. 2011, in IAU Symposium, Vol. 270, Computational Star Formation, ed. J. Alves, B. G. Elmegreen, J. M. Girart, & V. Trimble, 443–450

Juvela, M., Malinen, J., & Lunttila, T. 2012, A&A, 544, A141

Juvela, M., & Padoan, P. 1999, in Science with the Atacama Large Millimeter Array (ALMA)

Juvela, M., & Padoan, P. 2003, Astronomy & Astrophysics, 397, 201

Juvela, M., Pelkonen, V.-M., Padoan, P., & Mattila, K. 2008, Astronomy & Astrophysics, 480, 445

Juvela, M., Pelkonen, V.-M., & Porceddu, S. 2009, Astronomy & Astrophysics, 505, 663

Juvela, M., Ristorcelli, I., Pelkonen, V.-M., et al. 2011, Astronomy & Astrophysics, 527, A111

Karl, S. J., Naab, T., Johansson, P. H., et al. 2010, The Astrophysical Journal Letters, 715, L88

Krumholz, M. R., Klein, R. I., & McKee, C. F. 2007, The Astrophysical Journal, 665, 478

Kudoh, T., & Basu, S. 2011, The Astrophysical Journal, 728, 123

Landi Degl'Innocenti, E. 1976, Astronomy & Astrophysics Supplement Series, 25, 379

Lazarian, A. 2007, Journal of Quantitative Spectroscopy and Radiative Transfer, 106, 225

Leão, I. C., de Laverny, P., Mékarnia, D., de Medeiros, J. R., & Vandame, B. 2006, Astronomy & Astrophysics, 455, 187

Lehtinen, K., & Mattila, K. 1996, Astronomy & Astrophysics, 309, 570

Levermore, C. D., & Pomraning, G. C. 1981, The Astrophysical Journal, 248, 321

Li, A., & Draine, B. T. 2001, The Astrophysical Journal, 554, 778

Lis, D. C., & Menten, K. M. 1998, The Astrophysical Journal, 507, 794

Lombardi, M., & Alves, J. 2001, Astronomy & Astrophysics, 377, 1023

Lunttila, T., & Juvela, M. 2007, Astronomy & Astrophysics, 470, 259

—. 2012, Astronomy & Astrophysics, 544, A52

Lunttila, T., Padoan, P., Juvela, M., & Nordlund, Å. 2008, The Astrophysical Journal Letters, 686, L91

—. 2009, The Astrophysical Journal Letters, 702, L37

Mac Low, M.-M., & Klessen, R. S. 2004, Reviews of Modern Physics, 76, 125

Malinen, J., Juvela, M., Collins, D. C., Lunttila, T., & Padoan, P. 2011, Astronomy & Astrophysics, 530, A101

Mathis, J. S., Mezger, P. G., & Panagia, N. 1983, Astronomy & Astrophysics, 128, 212

Mathis, J. S., Rumpl, W., & Nordsieck, K. H. 1977, The Astrophysical Journal, 217, 425

Mattila, K. 1970, Astronomy & Astrophysics, 9, 53

—. 1980, Astronomy & Astrophysics Supplement Series, 39, 53

Mauron, N., de Laverny, P., & Lopez, B. 2003, Astronomy & Astrophysics, 401, 985

McKee, C. F., & Ostriker, E. C. 2007, Annual Review of Astronomy & Astrophysics, 45, 565

McKee, C. F., & Ostriker, J. P. 1977, The Astrophysical Journal, 218, 148

Mellema, G., Arthur, S. J., Henney, W. J., Iliev, I. T., & Shapiro, P. R. 2006, The Astrophysical Journal, 647, 397

Men'shchikov, A., André, P., Didelon, P., et al. 2010, Astronomy & Astrophysics, 518, L103

Mihalas, D. 1978, Stellar atmospheres (W. H. Freeman and Co.)

Mihalas, D., & Mihalas, B. W. 1984, Foundations of radiation hydrodynamics (Oxford University Press)

Mishchenko, M. I. 2008, Reviews of Geophysics, 46, 2003

Nakano, T., & Nakamura, T. 1978, Publications of the Astronomical Society of the Pacific, 30, 671

Ossenkopf, V. 1993, Astronomy & Astrophysics, 280, 617

Ossenkopf, V., & Henning, T. 1994, Astronomy & Astrophysics, 291, 943

Padoan, P., & Nordlund, Å. 1999, The Astrophysical Journal, 526, 279

—. 2002, The Astrophysical Journal, 576, 870

Pagani, L., Vastel, C., Hugo, E., et al. 2009, Astronomy & Astrophysics, 494, 623

Pelkonen, V.-M., Juvela, M., & Padoan, P. 2007, Astronomy & Astrophysics, 461, 551

Pilbratt, G. L., Riedinger, J. R., Passvogel, T., et al. 2010, Astronomy & Astrophysics, 518, L1

Pinte, C., Harries, T. J., Min, M., et al. 2009, Astronomy & Astrophysics, 498, 967

Planck Collaboration, Abergel, A., Ade, P. A. R., et al. 2011, Astronomy & Astrophysics, 536, A25

Porter, T. A., & Strong, A. W. 2005, in Proc. 29$^{\text{th}}$ International Cosmic Ray Conference (Pune), 77

Purcell, E. M. 1976, The Astrophysical Journal, 206, 685

Rees, D. E. 1969, Solar Physics, 10, 268

Rees, D. E., Durrant, C. J., & Murphy, G. A. 1989, The Astrophysical Journal, 339, 1093

Reid, M. J., & Silverstein, E. M. 1990, The Astrophysical Journal, 361, 483

Ritzerveld, J., & Icke, V. 2006, Physical Reviews E, 74, 026704

Robitaille, T. P. 2011, Astronomy & Astrophysics, 536, A79

Rosolowsky, E. W., Pineda, J. E., Foster, J. B., et al. 2008a, The Astrophysical Journal Supplement Series, 175, 509

Rosolowsky, E. W., Pineda, J. E., Kauffmann, J., & Goodman, A. A. 2008b, The Astrophysical Journal, 679, 1338

Rybicki, G. B., & Hummer, D. G. 1991, Astronomy & Astrophysics, 245, 171

Sault, R. J., Killeen, N. E. B., Zmuidzinas, J., & Loushin, R. 1990, The Astrophysical Journal Supplement Series, 74, 437

Scheffler, H., & Elsaesser, H. 1987, Physics of the galaxy and interstellar matter (Springer)

Schwartz, P. R. 1982, The Astrophysical Journal, 252, 589

Shu, F. H., Adams, F. C., & Lizano, S. 1987, Annual Review of Astronomy & Astrophysics, 25, 23

Siebenmorgen, R., Kruegel, E., & Mathis, J. S. 1992, Astronomy & Astrophysics, 266, 501

Skinner, C. J., Meixner, M., & Bobrowsky, M. 1998, Monthly Notices of the Royal Astronomical Society, 300, L29

Sousbie, T. 2011, Monthly Notices of the Royal Astronomical Society, 414, 350

Stahler, S. W., & Palla, F. 2005, The Formation of Stars (Wiley)

Steinacker, J. 2010, in Lecture Notes in Physics, Berlin Springer Verlag, Vol. 791, Lecture Notes in Physics, Berlin Springer Verlag, ed. J. Gracia, F. de Colle, & T. Downes, 117–136

Steinacker, J., Bacmann, A., Henning, T., Klessen, R., & Stickel, M. 2005, Astronomy & Astrophysics, 434, 167

Steinacker, J., Henning, T., & Bacmann, A. 2011, in IAU Symposium, Vol. 270, Computational Star Formation, ed. J. Alves, B. G. Elmegreen, J. M. Girart, & V. Trimble, 433–441

Steinacker, J., Pagani, L., Bacmann, A., & Guieu, S. 2010, Astronomy & Astrophysics, 511, A9

Stenflo, J. O. 1994, Solar Magnetic Fields - Polarized Radiation Diagnostics (Kluwer Academic Publishing)

Stepnik, B., Abergel, A., Bernard, J.-P., et al. 2003, Astronomy & Astrophysics, 398, 551

Struve, O., & Elvey, C. T. 1936, The Astrophysical Journal, 83, 162

Struve, O., & Story, H. 1936, The Astrophysical Journal, 84, 203

Surcis, G., Vlemmings, W. H. T., Curiel, S., et al. 2011, Astronomy & Astrophysics, 527, A48

Tassis, K., Dowell, C. D., Hildebrand, R. H., Kirby, L., & Vaillancourt, J. E. 2009, Monthly Notices of the Royal Astronomical Society, 399, 1681

Tassis, K., & Mouschovias, T. C. 2004, The Astrophysical Journal, 616, 283

Troland, T. H., & Crutcher, R. M. 2008, The Astrophysical Journal, 680, 457

Trujillo-Bueno, J., Moreno-Insertis, F., & Sanchez Martinez, F. 2002, Astrophysical Spectropolarimetry (Cambridge University Press)

Trumpler, R. J. 1930, Lick Observatory Bulletin, 14, 154

van Dishoeck, E. F., & Blake, G. A. 1998, Annual Review of Astronomy & Astrophysics, 36, 317

van Dishoeck, E. F., & Visser, R. 2011, ArXiv e-prints:1106.3917

Verschuur, G. L. 1968, Physical Review Letters, 21, 775

Walmsley, C. M., Flower, D. R., & Pineau des Forêts, G. 2004, Astronomy & Astrophysics, 418, 1035

Ward-Thompson, D., André, P., Crutcher, R., et al. 2007, Protostars and Planets V, 33

Ward-Thompson, D., Kirk, J. M., André, P., et al. 2010, Astronomy & Astrophysics, 518, L92

Weingartner, J. C., & Draine, B. T. 2001, The Astrophysical Journal, 548, 296

Williams, J. P., de Geus, E. J., & Blitz, L. 1994, The Astrophysical Journal, 428, 693

Witt, A. N., & Stephens, T. C. 1974, The Astronomical Journal, 79, 948

Witt, A. N., & Vijh, U. P. 2004, in Astronomical Society of the Pacific Conference Series, Vol. 309, Astrophysics of Dust, ed. A. N. Witt, G. C. Clayton, & B. T. Draine, 115

Wootten, A., & Thompson, A. R. 2009, IEEE Proceedings, 97, 1463